

Hurricane Superintensity

JOHN PERSING AND MICHAEL T. MONTGOMERY

Department of Atmospheric Science, Colorado State University, Fort Collins, Colorado

(Manuscript received 12 April 2002, in final form 17 October 2002)

ABSTRACT

High spatial and temporal resolution simulations using the Rotunno and Emanuel axisymmetric, cloud-resolving, hurricane model are found to greatly exceed Emanuel's energetically based upper bound for maximum potential intensity (E-MPI).

Using a control simulation similar to that of Rotunno and Emanuel with a sea surface temperature (SST) of 26.13°C, the E-MPI is exceeded after 15 simulation days, after the warming of the eye is able to extend down to the ocean surface. At still higher resolution, the modeled storm greatly exceeds E-MPI more quickly, during initial spinup, and the resulting intensity for the standard numerical and microphysical parameters is found to converge with, respectively, radial and vertical grid spacing of 3.75 km and 312.5 m with maximum tangential winds (V_{\max}) of $\approx 90 \text{ m s}^{-1}$. This is notably greater than the energetically based upper bound of $V_{\max} = 55 \text{ m s}^{-1}$. This "superintensity" occurs only in the presence of an enhancement of low-level eye entropy. The high-entropy air is entrained into the eyewall primarily by a breakdown of an azimuthal vortex sheet at the inner edge of the eyewall. Among the many underlying assumptions of E-MPI, only the violation of the related assumptions that the eyewall is neutral to moist ascent and that no entropy is fluxed from the eye to the eyewall can explain the degree of superintensity observed; other assumptions may be individually violated but their impacts on the intensity estimates are much smaller. The impact of the entrainment of heat from the eye to the eyewall on E-MPI theory is estimated through an ad hoc increase in the effective SST as a way of accounting for a second source of heat. This procedure produces a close estimate of the modeled intensity, but the problem is not closed since the degree of eyewall heating is not known a priori.

Published observations and recent three-dimensional, cloud-resolving modeling studies are reviewed that appear to present various aspects of the observed entropy structure and the eye-eyewall interaction of the superintensity mechanism.

1. Introduction

A complete investigation of hurricane intensity requires as a vital component (to paraphrase Emanuel 1988) an understanding of the processes that determine the upper bound on intensity. This upper bound, for a given set of environmental conditions, is the *maximum possible intensity*, customarily referred to as maximum potential intensity, or MPI. If an MPI principle can be found, then the manifold of possible intensities of the hurricane can be constrained. Camp (1999) provides an in-depth review of all the known theoretical approaches for constructing various MPI models.

Camp and Montgomery (2001) argue that the MPI theory of Emanuel "is the closest to providing a useful calculation of maximum intensity." This MPI theory was first introduced in Emanuel (1986, which shares some similarities to the approach of Kleinschmidt 1951) employing a frictional boundary layer beneath a con-

ditionally neutral outflow layer. Within this view, the energy for the storm comes from enhanced sea-to-air exchanges of enthalpy in the hurricane boundary layer due to enhanced wind speeds. The Emanuel (1986, 1988) theory, which was presented as a rigorous upper bound, and subsequent modifications [improved eye parameterization (Emanuel 1995b); inclusion of dissipational heating (Bister and Emanuel 1998)] will be referred to here as E-MPI. E-MPI theory has gained much acceptance in the community (Bosart et al. 2000; AMS Council 2000; Bengtsson 2001) and is widely considered a paradigm.

E-MPI is formulated on two-dimensional, axisymmetric principles, and neglects certain processes such as vertical wind shear (Jones 1995; Wang and Holland 1996; Frank and Ritchie 2001), convective asymmetries, spiral arm bands, vortex Rossby waves (Guinn and Schubert 1993; Montgomery and Kallenbach 1997; Schubert et al. 1999; Möller and Montgomery 2000; Chen and Yau 2001; Wang 2002a,b), ocean spray (Fairall et al. 1994; Andreas and Emanuel 2001), and wind-induced ocean cooling (Shay et al. 1998; Bender and Ginis 2000; Jacob et al. 2000). Given these simplifications, one might anticipate that E-MPI can only serve

Corresponding author address: Dr. John Persing, Dept. of Atmospheric Science, Colorado State University, Fort Collins, CO 80523-1371.

E-mail: john@eady.atmos.colostate.edu

as an approximate upper bound on real hurricanes that are three-dimensional and include all of these unmodeled processes. On the other hand, in an axisymmetric computer model that has a simplified one-way ocean–air interaction one might anticipate that E-MPI could be an exact upper-bound on the intensity of the resulting axisymmetric storms. Indeed, E-MPI theory was previously “validated” against results from such axisymmetric models (Rotunno and Emanuel 1987; Emanuel 1989, 1995a).

Using a nonhydrostatic, many-layered, axisymmetric hurricane model (based on Ooyama 2001) with standard tropical parameters, Hausman (2001) recently demonstrated a systematic increase of storm intensity with model resolution, with convergence found at approximately 1 km horizontal grid spacing [using 28°C sea surface temperature (SST)] with a maximum sustained tangential velocity of 140 m s⁻¹. Needless to say, this *greatly* exceeds the E-MPI for this model storm with any reasonable estimation of an outflow temperature from a Jordan (1958) mean sounding. It is worth noting that, long ago, Yamasaki (1983) reported an axisymmetric simulation with >90 m s⁻¹ with 28.85°C SST that also exceeds E-MPI. Because of these findings and the fundamental nature of the problem, we believe a reexamination and a more thorough testing of E-MPI theory is warranted.

This paper will demonstrate a hitherto unreported resolution sensitivity in the Rotunno and Emanuel (1987) model that results in a hurricane vortex that greatly exceeds E-MPI. To explain the simulated phenomenon, we examine each of the assumptions of E-MPI and find that the underlying philosophy of E-MPI, namely that there exists a point balance of entropy and angular momentum at the top of the subcloud layer at the base of the eyewall, cannot explain the observed “superintensity.” We will show that the addition of heat from the eye to the eyewall, which violates two key assumptions of E-MPI (that there is no such interaction and that the eyewall is neutral to moist ascent), is responsible for the enhanced wind speeds.

The plan of the paper is as follows. Section 2 briefly reviews the Rotunno and Emanuel 1987 model and our numerical experiments with it. Section 3 briefly reviews E-MPI. Section 4 documents the behavior of high-resolution simulations that produce very intense storms compared to E-MPI. Section 5 documents the evolution of air with high entropy in the simulated eye and demonstrates that this air interacts with the eyewall. Section 6 provides evidence that the pertinent element of the eye–eyewall interaction is as a source of latent heat rather than of local buoyancy. Section 7 provides supporting evidence of the superintensity mechanism from observations and recent three-dimensional cloud-resolving simulations. Section 8 provides a discussion. Section 9 presents our conclusions.

2. Rotunno and Emanuel model reviewed

The Rotunno and Emanuel (1987, hereafter RE87) hurricane model is an axisymmetric (two-dimensional), nonhydrostatic, cloud-resolving version of the Klemp and Wilhelmson (1978) formulation originally developed for the study of cumulus clouds and supercell storms. This model was kindly provided to us by R. Rotunno of the National Center for Atmospheric Research (NCAR). The model is integrated on a staggered C grid using a fixed radial and fixed vertical grid spacing. There is no ice in the model and explicit convection is employed with a fixed precipitation fallspeed of 7 m s⁻¹. Subgrid-scale turbulence is parameterized using a standard Smagorinsky (1963) formulation modified to allow a variable mixing length, a function of the local stability using a Richardson-number-dependent closure following Lilly (1962). Radiation is represented crudely by a standard Newtonian cooling parameterization that tends to restore the local potential temperature to that found initially in the ambient environment. In the numerical experiments presented here the radiational heating/cooling rate is capped at 2 K day⁻¹. Sponge layer damping occurs above the model tropopause ($z > 19.4$ km). The outer boundary at $r = 1500$ km is open; using a doubled radius for the outer boundary does not give significantly different results. Surface interaction is through a standard bulk aerodynamic parameterization. The surface drag coefficient C_D is represented by a linear function of wind speed using Deacon’s formula (Roll 1965). The surface enthalpy exchange coefficient C_k is set equal to the drag coefficient ($C_k/C_D = 1$). The radial and vertical wind fields (u and w , respectively) are computed using a “fast” time step to handle sound waves. All of these processes are unchanged from those described in RE87. The initial thermodynamic sounding of the environment is created by a procedure described in RE87 as a modification of the Jordan (1958) sounding so that it is neutral to convection as realized in the model.

Model parameters used in the default run are summarized in Table 1. These are the same as experiment A in RE87 except there the SST reported is 26.3°C¹ and the radiational cooling is uncapped.² For each doubling of model resolution, the time step is halved, the number of radial and vertical grid points is doubled, the number of integration steps is doubled, and the initial soundings of potential temperature (θ) and vapor mixing ratio (q_v) are interpolated to the new vertical grid. As a consequence of these changes, the radial and vertical grid

¹ SST in the RE87 model is a weak function of pressure and we report a typical SST found under the eyewall.

² The cooling used here is that found in experiment J (2 K day⁻¹) of RE87. This experiment was found by RE87 to have overall structure similar to experiment A (their control; unbounded Newtonian cooling) and was 5 m s⁻¹ more intense than experiment A. RE87 found these intensity changes to be consistent with MPI theory because of changes in T_{out} .

TABLE 1. Default run settings.

Number of radial v points	NR = 100
Number of vertical v points	NZ = 20
Outer boundary	$R_0 = 1500$ km
Upper boundary	$z_{\text{top}} = 25 \times 10^3$ m
Radial grid spacing	$\Delta r = R_0/\text{NR} = 15$ km
Vertical grid spacing	$\Delta z = z_{\text{top}}/\text{NZ} = 1250$ m
First sponge-layer grid level	$I_{\text{spn}} = 16$
Simulation run time	$t_{\text{end}} = 30$ days
Time step (long)	$\Delta t = 20$ s
Time step (short)	$\Delta t_s = \Delta t/5 = 4$ s
Coriolis parameter	$f = 5 \times 10^{-5} \text{ s}^{-1}$
Coefficient of drag at $V = 0$	$C_{D_0} = 1.1 \times 10^{-3}$
Ratio of coefficients of exchange	$C_k/C_D = 1.00$
“Total” mixing length	$l = 200$ m
“Horizontal” mixing length	$l_h = 0.2 \times \Delta r = 3$ km
Initial V_{max}	12.7 m s^{-1}
Initial radius of max winds	$\text{RMW}_i = 82.5$ km
Initial outer radius of vortex	$r_{oi} = 412.5$ km
Initial ocean potential temperature	$\theta_{s_i} = 298$ K
Ambient surface pressure	$p_{\text{amb}} = 1015.1$ mb
Ocean temperature	$T_s = 299.2$ K = 26.13°C

spacings are halved, the fast time step is halved, and the horizontal mixing length is halved. Simulations will be referred to as the “default run,” “2x run,” “4x run,” and “8x run” with each doubling of radial, vertical, and temporal resolution. For the presentation of results, days (8.64×10^4 s) are used, with the simulations starting at day 0. Figure 1 shows that the 4x run produces a realistic hurricane vortex like Fig. 5 of RE87, except that it is more structured and much more intense, possessing stronger updrafts.

3. E-MPI theory reviewed

a. Foundations

The energetically based MPI theory considered here is that first presented by Emanuel (1986) and updated with an improved representation of the eye in Emanuel (1995b, hereafter E95b) yielding a minimum surface pressure that depends explicitly on the ratio of exchange coefficients of enthalpy and angular momentum. Camp and Montgomery (2001) provided a summary of E-MPI and its physical basis. Bister and Emanuel (1998) updated E-MPI to include the effects of dissipational heating in the boundary layer, but since the model results presented here do not include this process the theory of E95b will be considered.

The basic functional form of E-MPI is

$$V_{\text{max}} = V_{\text{max}}(T_s, T_{\text{out}}, \mathcal{H}; p_{\text{amb}}, f, r_0), \quad (1)$$

where the maximum tangential wind V_{max} is a function of the SST (T_s), the outflow temperature (T_{out} ; defined precisely in section 4 below), and the surface relative humidity (\mathcal{H}) which is assumed to have the same value at the eyewall as in the environment. *Since the thermal wind relation is central to the derivation and is not valid in the boundary layer, V_{max} must refer to the value at the top of the boundary layer.* E-MPI is also a weak

function of the ambient surface pressure p_{amb} , latitude through the Coriolis parameter f , and the size of the vortex where r_0 is the radius at which surface tangential winds vanish. In dimensional terms, Eq. (16) of E95b becomes

$$V_{\text{max}}^2 = \frac{C_k}{C_D} \frac{\left(\chi_{si}^* - \frac{1}{4} \gamma^* r_0^2 f^2 \right)}{\left(1 - \frac{1}{2} \frac{C_k}{C_D} \gamma^* \right)}, \quad (2)$$

where C_k/C_D is the ratio of the boundary layer exchange coefficients of enthalpy and angular momentum and is taken to be unity throughout this paper. The entropy variable χ has the units of energy per unit mass (i.e., squared velocity) and is defined by

$$\chi = (T_s - T_{\text{out}})(s - s_{bi}), \quad (3)$$

where $s = c_p \ln \theta_e$ is the moist entropy, s_{bi} is the initial ambient boundary layer value of moist entropy, c_p is the specific heat of dry air at constant pressure, and θ_e is the equivalent potential temperature (e.g., Holton 1992) which is conserved in pseudoadiabatic ascent. In (2), the parameter

$$\gamma^* = A \frac{1 - \mathcal{H}}{1 - \mathcal{H}A}, \quad (4)$$

where

$$A = \frac{T_s - T_{\text{out}}}{T_s} + \frac{\chi_{si}^*}{R_d T_s (1 - \mathcal{H})} \quad (5)$$

and χ_{si}^* is saturation χ evaluated at the ocean surface and at ambient surface pressure, and R_d is the gas constant of dry air. Equations (2)–(5) are a closed expression for V_{max} , and the solution is found to be largely insensitive to large, but reasonable, variations in r_0 and p_{amb} (e.g., E95b). Figure 2 shows the solution in terms of V_{max} as a function of T_s and T_{out} for $\mathcal{H} = 80\%$, $p_{\text{amb}} = 1015.1$ mb, $f = 5 \times 10^{-5} \text{ s}^{-1}$, and $r_0 = 400$ km. This figure provides a baseline against which high-resolution, cloud-resolving simulations can be compared.

b. Boundary layer balances

Evaluation of \mathcal{H} is problematic in the diagnosis of the RE87 model output (see appendix). Relative humidity is introduced into the derivation to close the vertical entropy gradient between the boundary layer and the ocean surface and to join the solution at the eyewall with that in the environment (where values might be known in practice prior to cyclogenesis from either climatology or routine data acquisition). By appealing to an earlier step in the derivation of E-MPI [Eq. (13) from E95b], we can derive a “local” expression for the tangential velocity at the top of the boundary layer as a function of radius:

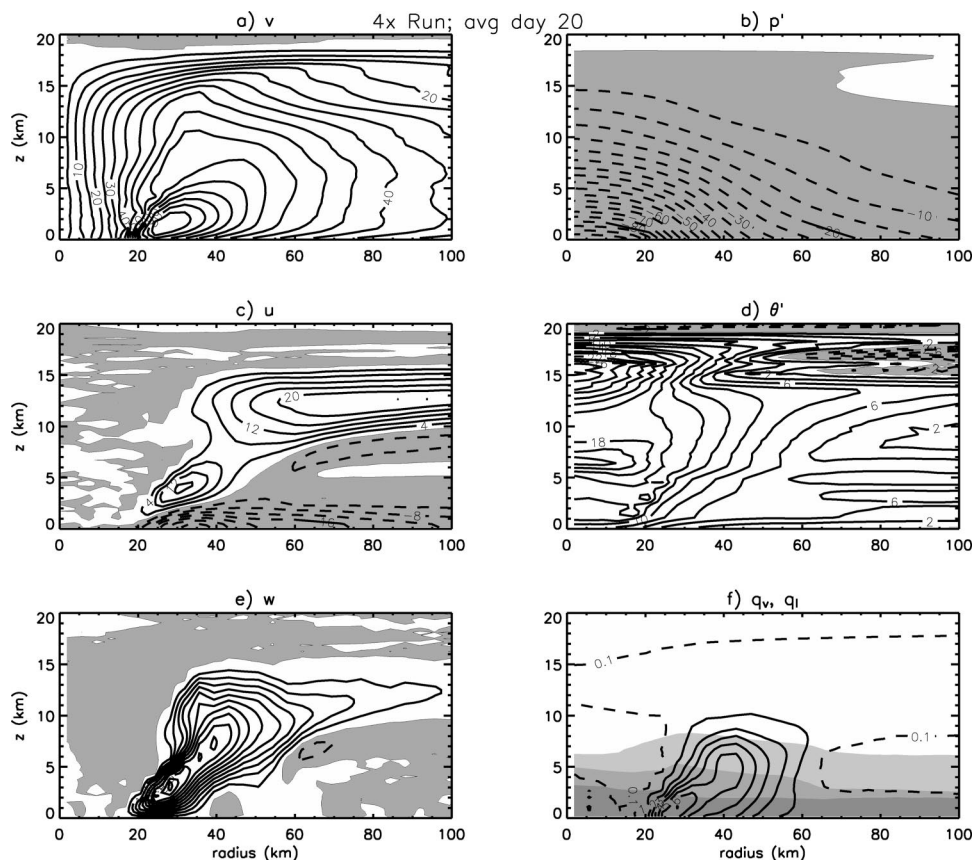


FIG. 1. The 20.0–21.0-day average fields in the 4x run near the eyewall. (a)–(e) Shaded regions indicate negative values of the field: (a) tangential velocity (contour interval is 5 m s^{-1}); (b) dimensional pressure deviation from the outer boundary (at 1500-km radius; contour interval is 5 mb); (c) radial velocity (contour interval is 4 m s^{-1}); (d) potential temperature deviation from the initial state (contour interval is 2 K); (e) vertical velocity (contour interval is 0.5 m s^{-1}); (f) liquid water mixing ratio (contour interval is 1 g kg^{-1}); dashed line denote the 0.1 g kg^{-1} contour and water vapor mixing ratio; lightest shading indicates $3 < q_v < 8 \text{ g kg}^{-1}$; darker shading indicates $8 < q_v < 13 \text{ g kg}^{-1}$; darkest shading indicates $q_v > 13 \text{ g kg}^{-1}$.

$$V_{\text{Estimated}}^2(r) = \frac{C_k}{C_D} [\chi_s^*(r) - \chi_b(r)]. \quad (6)$$

Here, χ_s^* is the saturation entropy at SST, which is a function of radius because of the radial variation in surface pressure, and χ_b is the local entropy variable defined at the top of the subcloud layer and is taken to be representative of the full depth of a well-mixed boundary layer. Thus, the squared velocity is proportional to the vertical difference of entropy across the boundary layer. This expression should be valid for the eyewall of a steady-state storm where $\chi_b(r)$ is maintained by a balance between loss due to radial advection by the inflow and gain from the underlying ocean, and angular momentum is locally maintained as a balance between frictional loss to the ocean and spinup due to inward flux of environmental angular momentum. The expression is only valid at high cyclonic wind speeds and at small radii such as that found near the eyewall. Equation (6) could not serve as a practical MPI [cf. Eq. (2)] because the parameters cannot be determined before a

storm forms; it nevertheless serves as a diagnostic of the accuracy of many assumptions (see appendix for a summary) used to derive E-MPI. In particular, estimation of relative humidity is problematic in the model output, but (6) dodges this problem and provides an estimate of E-MPI that is only weakly dependent on resolution. Differences between (6) and (2) largely reflect errors in the closure assumptions used to derive (2).

c. A model-appropriate θ_e

Moist entropy is conserved under moist adiabatic ascent because phase changes represent reversible exchanges of energy between a latent potential of vapor and internal energy of the mixed gases of air. It is necessary for this paper to use a form of equivalent potential temperature that the axisymmetric numerical model approximately conserves (RE87, p. 544):

$$\Theta_e = \theta + \frac{L}{c_p T} q_v. \quad (7)$$

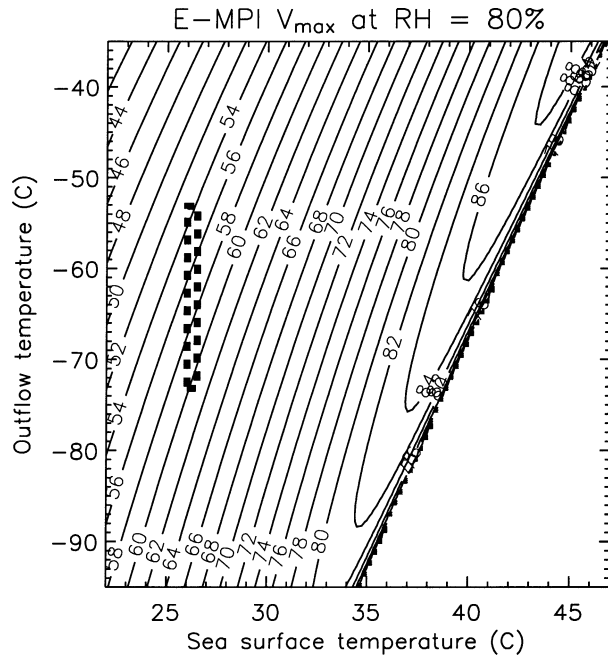


FIG. 2. V_{\max} from E-MPI as a function of T_s and T_{out} . The boxed area denotes the range of values found in the present paper.

This form of θ_e is used throughout this paper where RE87 results are concerned. This underestimates the commonly used exponential form (e.g., Holton 1992, p. 289)

$$\theta_e = \theta \exp\left(\frac{Lq_v}{c_p T}\right), \quad (8)$$

and the empirically computed form of Bolton (1980, p. 1052)

$$\theta_e = \theta \exp\left[1000q_v(1 + 0.81q_v)\left(\frac{3.376}{T} - 0.00254\right)\right] \quad (9)$$

by up to 10% (5 K) and 20% (10 K), respectively, of the magnitude of the last term of (7) in moist tropical environments.

4. Superintensity

The phenomenon in which axisymmetric hurricane models tend to form more intense storms with increasing model resolution was reviewed by Hausman (2001) and was supplemented by his own simulations using a new thermodynamic formulation by Ooyama (2001). For a 28°C SST simulation at the highest resolution employed ($\Delta r = 500$ m) without ice physics, the intensity of the modeled hurricane reached 140 m s⁻¹. Inclusion of ice physics was found to weaken the storm intensity somewhat (120 m s⁻¹), but since this process is not included in E-MPI theory, the subject of our comparison, the

simulations lacking ice are the most appropriate for comparison with E-MPI and the RE87 model simulations presented here. This sensitivity to resolution is confirmed here with the entirely different RE87 model (Fig. 3), where the modeled intensity (solid curves) greatly exceeds E-MPI [Eq. (2); dotted curves]. The overlays on Fig. 3 are estimated using daily averaged data. The dashed curves [using Eq. (6), evaluated at the lowest grid level at the radius of maximum winds (RMW)] show a slight increase with increasing intensity, but not nearly enough to explain the modeled superintensity. Use of (6) in this manner does justify in part the use of a fixed \mathcal{H} in (2), otherwise using model output estimates of \mathcal{H} (2) would provide weaker estimates of intensity with increasing resolution (see appendix for more on this point). The tendency to greatly exceed E-MPI ($V_{\max} \gg V_{\text{E-MPI}}$) at high resolution will hereafter be referred to as *superintensity* and will be the focus of the remainder of this paper.

Run	Default	2x	4x	8x
MAX(V) (m s ⁻¹)	71.77	87.74	100.20	101.90
MAX[D(V)] (m s ⁻¹)	67.81	83.75	95.96	96.79
MEDIAN(V) (m s ⁻¹)	62.04	80.21	90.42	87.51
MEAN(R) (km)	43.89	22.23	26.14	22.91
MIN(P) (mb)	935.0	906.5	894.2	901.8
MEDIAN(P) (mb)	952.9	917.7	910.1	922.9
MAX(W) (m s ⁻¹)	8.32	13.20	22.80	30.13
MAX[D(W)] (m s ⁻¹)	4.77	7.58	10.86	13.58

The 2x, 4x, and 8x runs appear to reach a quasi-steady-state intensity by 10 days, with generally stronger steady-state intensities at higher resolution. The default case (Fig. 3a) also appears to complete its initial spinup by day 10, but slowly transitions to a second apparent steady state near 20 days. Table 2 summarizes the output from each model run. From the first three rows we see evidence for convergence in the ultimate quasi-steady-state vortex intensity with increases in resolution by the 4x run. While MAX(V) and MAX[D(V)] continue to increase slightly for the 8x run, these can be attributed to short-lived events on the order of a day (Fig. 3). MEDIAN(V) for the 8x run is actually smaller than for the 4x run. The “typical” quasi-steady-state intensity can then be considered about the same for the 4x and 8x runs. Hausman (2001) proposed that, at higher resolution, a smaller RMW is resolvable and will result because the limiting factor is the ability of numerical diffusion to mix low angular momentum air outward from the center of the storm, a process whose spatial scale is on the order of

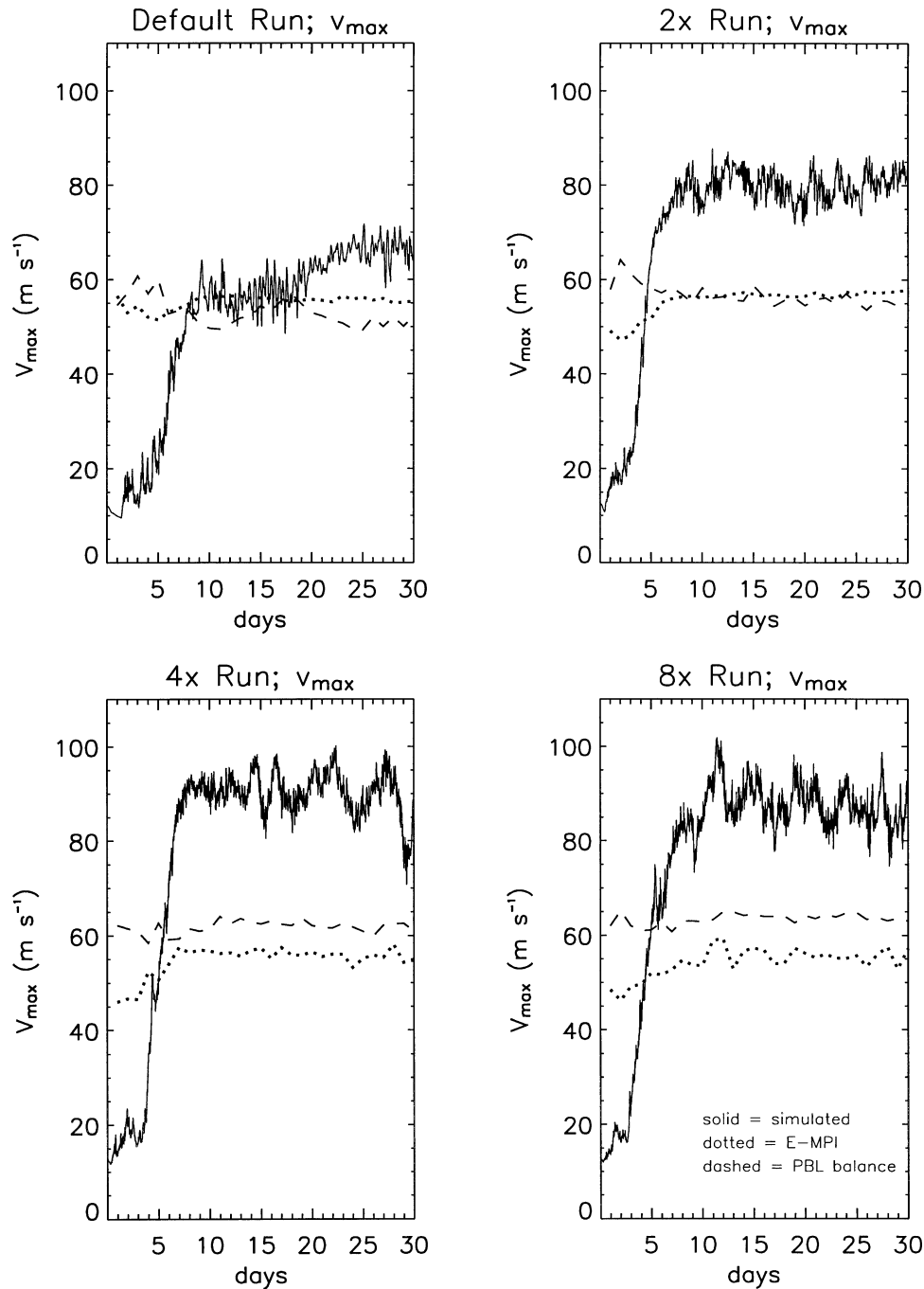


FIG. 3. Time series of maximum tangential winds for the (a) default, (b) 2x, (c) 4x, and (d) 8x runs. Overlaid are theoretical predictions of maximum intensity using E-MPI (dotted) from Eq. (2) (with a fixed 80% RH) and using a boundary layer balance (dashed) from Eq. (6) evaluated at the RMW. The overlays are computed once daily using daily averaged model output.

the grid scale. Because the RMW is found to be the approximate limit for inward advection of environmental angular momentum, a smaller RMW at higher resolution was hypothesized to be the primary control for maximum intensity of the model hurricane in Hausman (2001). From our default and 2x runs, $MEAN(R)$ is

about $3\Delta r$, but $MEAN(R)$ does not become systematically smaller at higher resolution, and the observed difference in steady-state intensity between the 2x and 4x runs cannot be explained solely by a change in RMW. Although the 4x run appears most intense in terms of central pressure, $MEDIAN(P)$ seems also to have largely

converged by the 2x run at about 915 mb. Both extreme updrafts, MAX(W), and the “smoothed” peak updrafts MAX[D(W)] appear not to have converged with these simulations.

The outflow temperature for Fig. 3 should be computed following a parcel using

$$T_{\text{out}} = \frac{1}{\ln \frac{\theta_{e_a}}{\theta_e}} \int_{\ln \theta_e}^{\ln \theta_{e_a}} T d(\ln \theta_e). \quad (10)$$

This equation follows that of RE87, except with a reversed order of integration so that the direction of the integral is in the same direction as the transverse flow. In (10) the integral begins at the base of the updraft in the eyewall and terminates at an ambient value θ_{e_a} where the parcel comes in contact again with the boundary layer.³ This proved expensive to compute in practice and frequently the computed trajectories intersect the outer boundary making evaluation impossible. For convenient computation, the form of T_{out} used in Fig. 3 is an outflow-weighted temperature (i.e., the typical temperature of air exiting the hurricane) evaluated at $r = 150$ km computed using daily averaged fields

$$T_{\text{out}} = \left(\frac{1}{\int_{z=0}^{z_{\text{top}}} U^{(+)} dz} \right) \int_{z=0}^{z_{\text{top}}} U^{(+)} T dz, \quad (11)$$

where

$$U^{(+)} = \begin{cases} 0 & \text{for } u < 0 \\ u & \text{for } u \geq 0. \end{cases} \quad (12)$$

Because the integral in (10) includes portions of the middle and lower troposphere, which are not strongly weighted in (11), we should expect using simple lapse rate considerations (11) to give a somewhat cooler estimate of (10). For our cases it appears as a cool bias of 5–10 K. Supplying this bias into E-MPI provides for a 5 m s^{-1} strong bias in estimating V_{max} .

5. The eye as a latent heat reservoir

a. Phenomenological evidence

The hypothesis of this paper, namely that a beneficial interaction between the eyewall and warm, moist air in the low-level eye permits modeled storm intensities that greatly exceed E-MPI, is motivated by the behavior of the default run before and after 20 days, when the transition from one quasi-steady intensity to another occurs (Fig. 3a). Prior to day 18 there is a θ anomaly ($\theta - \theta_{\text{initial}}$) in the boundary layer of the eye (RMW at the surface ~ 40 km), but almost no temperature anomaly

($T - T_{\text{initial}}$; Fig. 4). After this time, warming is sufficient to increase the temperature near the surface as well. The higher-resolution simulations show this fully developed eye structure during the initial contraction of the vortex (before 10 days), and thus do not pass through multiple intensity states. Associated with this eye structure is an enhancement of Θ_e in low levels. In the case of the default run, the low-level eye Θ_e is a relative maximum near $r = 20$ km, $z = 3$ km on day 18 (Fig. 5). Because this enhanced Θ_e (Liu et al. 1999), if introduced into the convectively modified environment of the eyewall, can represent a source of local heat, this feature can be referred to as a reservoir of potential heat.

The establishment of the reservoir in our default run appears to occur in two steps. The first step involves the elimination of the initial midlevel Θ_e minimum. By day 6, the minimum has been pinched in half near $r = 40$ km with the development of persistent convection in the eyewall. This persistent convection equilibrates the eyewall close to a moist adiabat by day 8 (Fig. 5). After the convection is established, a secondary circulation is created in the eye that forces descent and recirculation into the eyewall at low levels [Gray (1998) notes the angular momentum impact of such an interaction]. This eye circulation advects the original Θ_e minimum to lower levels where it can come into contact with the top of the boundary layer and can be modified by the ocean. Surface fluxes then eradicate the Θ_e minimum, but by day 18 the vertical Θ_e gradient is reversed. The descent also advects down the high Θ_e (interchangeably θ with small q_v) that defines the tropopause. This warms the eye (Gray 1998).

At higher resolution, a multiscale response of the eye can now be resolved, with strong descent concentrated in a narrow column just interior to (i.e., at smaller radii than) the eyewall, with much weaker descent throughout the rest of the eye (e.g., Willoughby 1998). Because of this, the original midlevel Θ_e minimum is never totally eliminated from the eye (Fig. 6). On the other hand, Θ_e is locally enhanced just interior to the eyewall, which results from a combination of dry descent and subgrid-scale inward mixing (which is locally nonconservative) of vapor from the saturated eyewall. The channel of warmest Θ_e at day 10 is also under weak saturated ascent, interior to the peak updraft. By day 10, the 360-K contour connected to the upper troposphere descends down to 3 km. After this time this contour ascends and the lower-level reservoir appears to expand with the 360-K contour moving up to 5-km altitude. This occurs as a result of both an inward radial diffusion of vapor and vertical advection of heat and moisture from the eye boundary layer, which is enriched by interaction with the ocean. The default run ($\Delta r = 15$ km), which resolves the eye by one or two radial grid points, cannot represent this detailed circulation.

The ultimate source of enhanced entropy for the low-level eye in the 4x run is an upward flux of moisture from the ocean surface at greatly reduced surface pres-

³ This represents the “cold” reservoir temperature of the Carnot cycle presented in Emanuel (1986) assuming ascent in the eyewall preserves its value of θ_e .

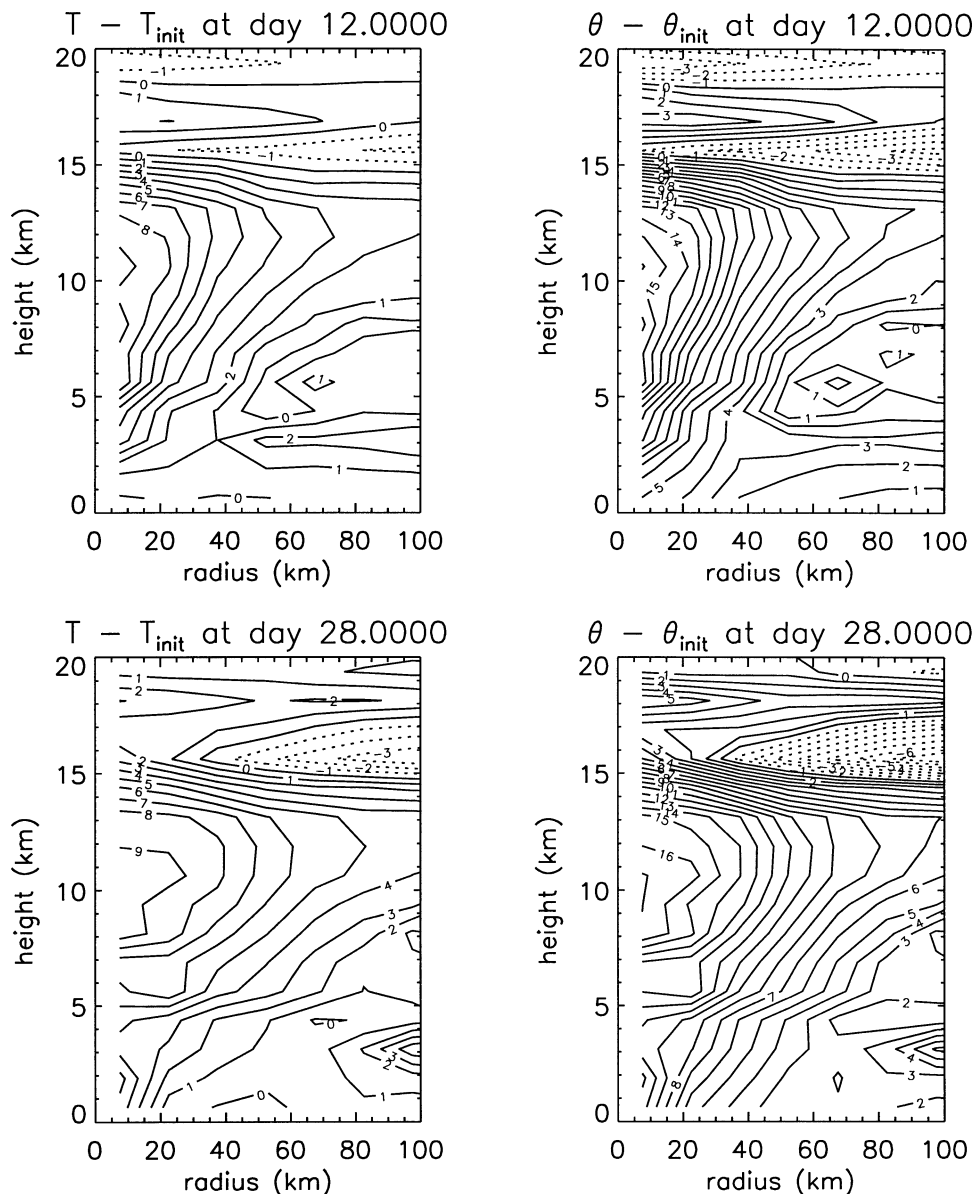


FIG. 4. Temperature T and potential temperature θ (K) from the default run displayed as departures from the initial state for days 12 and 28.

sure (Fig. 7), in contrast to the default case, which has a much weaker latent heat reservoir. The warming of the eye has led to a reversal of the vertical potential temperature gradient such that the eye is actually warming the ocean. However, subsaturation in the eye leads to a much greater flux of q_v into the atmosphere. The net effect is to positively force Θ_e . A negative flux removing moist entropy from the low-level eye is therefore necessary to maintain a steady state. Smith (2003) presents an idealized boundary layer model for hurricane-like vortices and finds the boundary layer remains subsaturated. For his cases, the surface latent heat flux is maximized at the RMW, but is also significantly positive beneath the eye, like that found in Fig. 7.

b. Lagrangian trajectories

To confirm whether the eyewall updraft is being affected by warm, moist air from the eye, forward/backward Lagrangian trajectories bisecting the eyewall updraft are computed and displayed in Figs. 8 and 9. These are “seeded” at day 24.4 of the 4x run across the updraft at the 2-km height at equal radial spacing and are calculated forward for 0.1 day and backward for 0.4 day. Figure 8 shows that there are three subjectively identified source regions for air upon introduction to the eyewall updraft: 1) the boundary layer inflow (solid), 2) low-level inflow above the boundary layer (dashed), and 3) the eye (dotted). Selection of a higher seeding

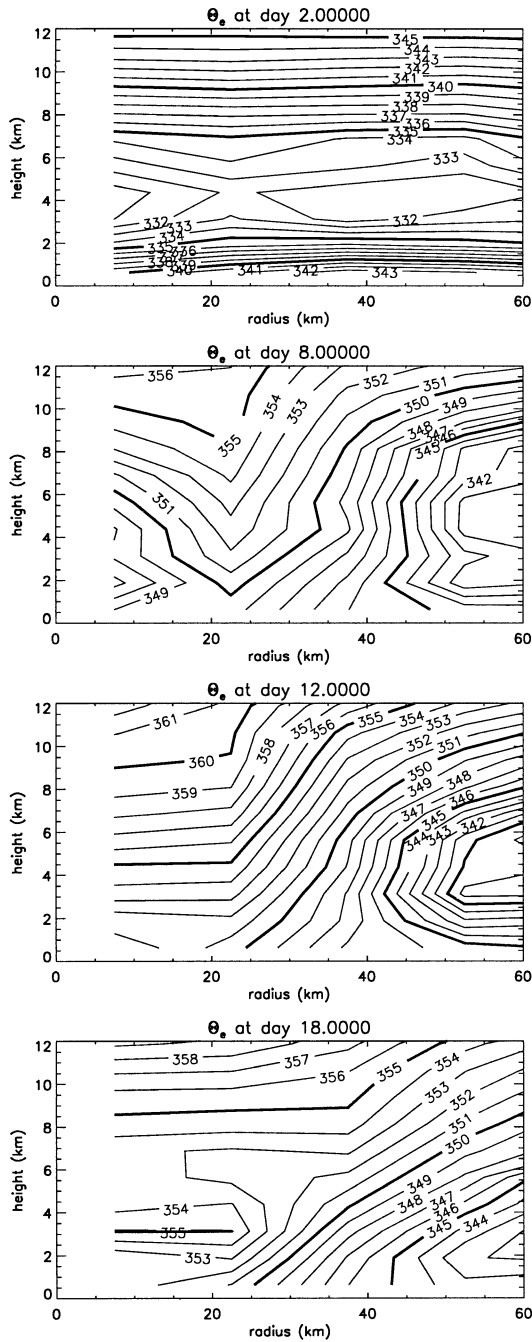


FIG. 5. Equivalent potential temperature Θ_e (K) at various times in the default run.

altitude can also expose a midlevel ($z \approx 5$ km) inflow (not shown). Of the inflow parcels shown here (Fig. 8; solid and dashed), some originate from a downdraft of a convective feature near $r = 45$ km and others from the boundary layer inflow from further radii. A similar feature was found by Braun (2002) using trajectories in a three-dimensional simulation of Hurricane Bob (1991; reproduced here as Fig. 10).

Figure 9 shows that the entropy of the downdraft

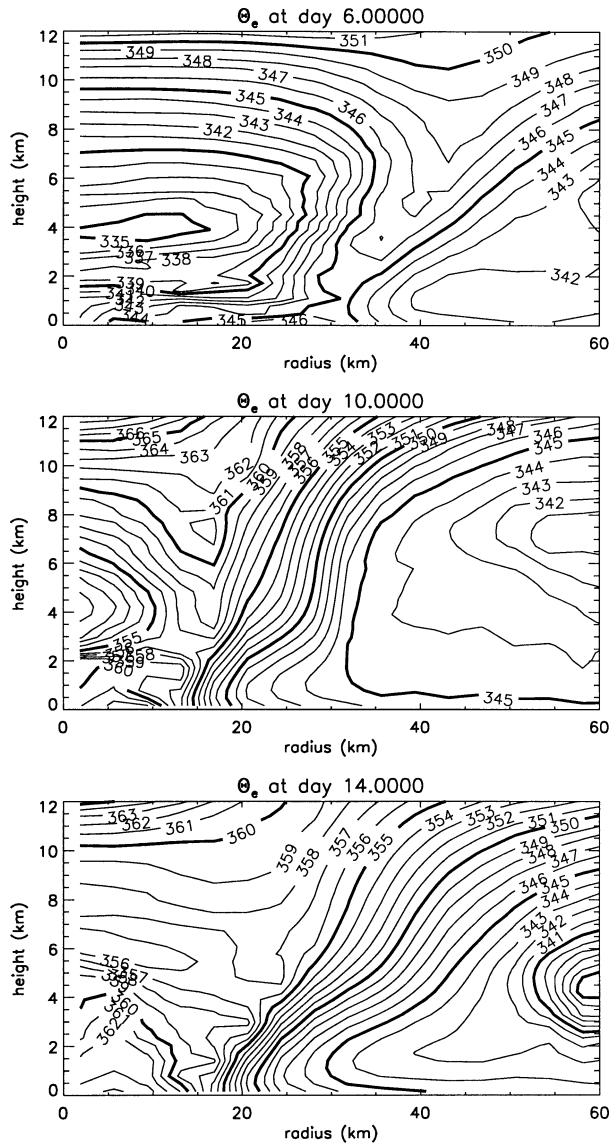


FIG. 6. Equivalent potential temperature Θ_e (K) at various times in the 4x run.

trajectories is indistinguishable from the other inflow trajectories (solid and dashed) by the time they encounter the eyewall updraft. The general nature of these trajectories (Fig. 9) are quite similar to trajectories shown by Braun (2002) in Fig. 10c. The Θ_e of the inflow trajectories is mostly a function of their originating height, and as they enter the eyewall, lower trajectories warm even more while penetrating to smaller radii (similar to Braun 2002). This is entirely consistent with a dominant ocean interaction. A handful of boundary layer inflow trajectories obtain much greater Θ_e values (355 K or more; lower-right part of Fig. 9, dotted) as they enter the base of the eye; typically the radial inflow weakly extends to the center of the storm due to the Ekman pumping in the weak positive vorticity regime

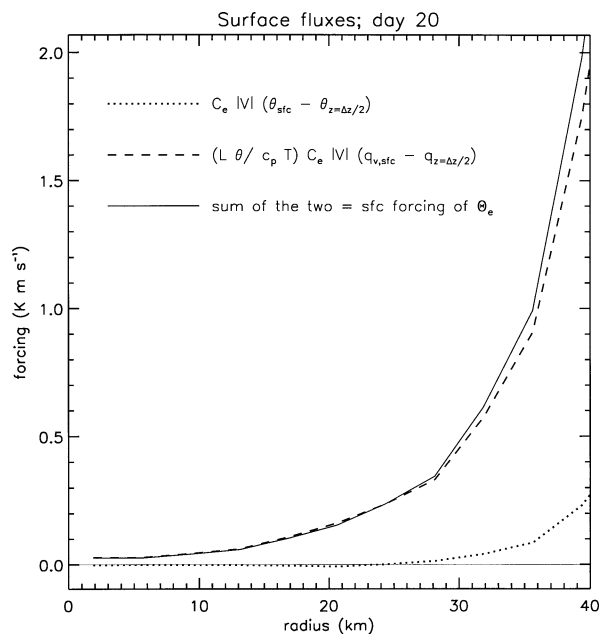


FIG. 7. Surface forcing terms from the 4x run.

of the eye. These penetrating inflow trajectories linger up to 2 h in the eye before being introduced into the eyewall updraft. The left-to-right traces of trajectories in Fig. 9 (dotted) indicate mixing of entropy with neighboring air. Boundary layer inflow trajectories increase in entropy as they ascend in the eyewall updraft to $z = 2.5$ km. Since much of this increase occurs above the boundary layer, an exchange of entropy must result from an additional source of warm Θ_e other than the ocean, namely the eye.⁴ Above $z = 2.5$ km, trajectories ascending in the outer portion of the eyewall continue to increase in Θ_e , while those in the inner portion first decrease in Θ_e below $z = 4.5$ km (indicative of an exchange of entropy within the eyewall) and increase again above this level. Braun (2002) reached a similar conclusion with three-dimensional trajectories, suggesting that the results presented here are not peculiar to axisymmetric geometry. Parcels located near the inner edge of the eyewall detrain into the eye, where they increase in Θ_e , and frequently are reintroduced into the eyewall at a later time.

Based on the foregoing results, we can suggest that two related assumptions of E-MPI are violated in this model: the entropy exchange from the eye to the eyewall is nontrivial (which is confirmed with an Eulerian Θ_e budget that is not shown here) and the eyewall updraft is not moist neutral. The violation of moist neutrality is a consequence of a beneficial turbulent entrainment into the eyewall of high latent heat air from the low-level eye.

⁴ In the saturated eyewall, Θ_e is no different from its value at saturation, and both are conserved in pseudoadiabatic ascent.

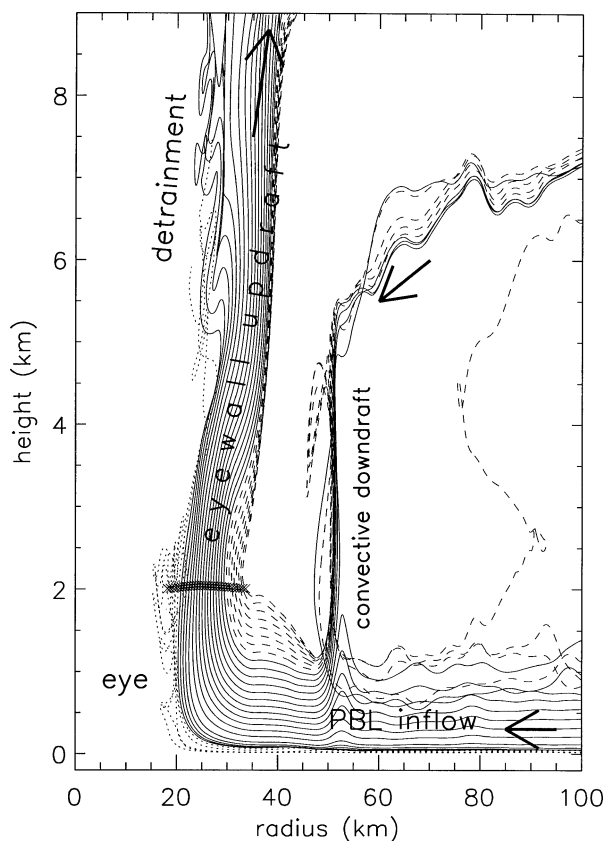


FIG. 8. Half-day trajectories (when contained within the display domain) from the 4x run. These are forward/back trajectories seeded at 24.40 days at a height of 2 km, bisecting the eyewall draft at equal spatial intervals. Trajectories are computed forward for 0.1 days and backward 0.4 days using the same seed points. Dotted trajectories enter the eyewall from the eye; solid trajectories enter the eyewall from the boundary layer inflow; dashed trajectories enter the eyewall from above the boundary layer; Xs mark the seeding locations.

c. Experimental suppression of the reservoir

To confirm that the low-level entropy source in the eye is crucial for maintaining the hurricane at superintensity, we might propose to eliminate the source through some artificial means. An experiment was performed where enhanced cooling by Newtonian relaxation (our surrogate for radiation; 8 K day^{-1}) was applied in the lower eye after day 15 of the 4x run. This leads to a rapid reduction of storm intensity from 90 to 75 m s^{-1} (not shown), but the intensity stabilized above E-MPI (55 m s^{-1}). This occurred because the RMW expanded from 20 to 30 km, thus placing 10 km of radial separation between the eyewall and our imposed forcing (Fig. 11). This experimental run produced a radial displacement of the latent heat reservoir centered on $r = 25$ km (compared to the control experiment where the reservoir is nominally centered at the origin). While E-MPI does not explicitly depend on the RMW, the expansion of the RMW could in part explain the weakening. On the other hand, the displaced entropy reser-

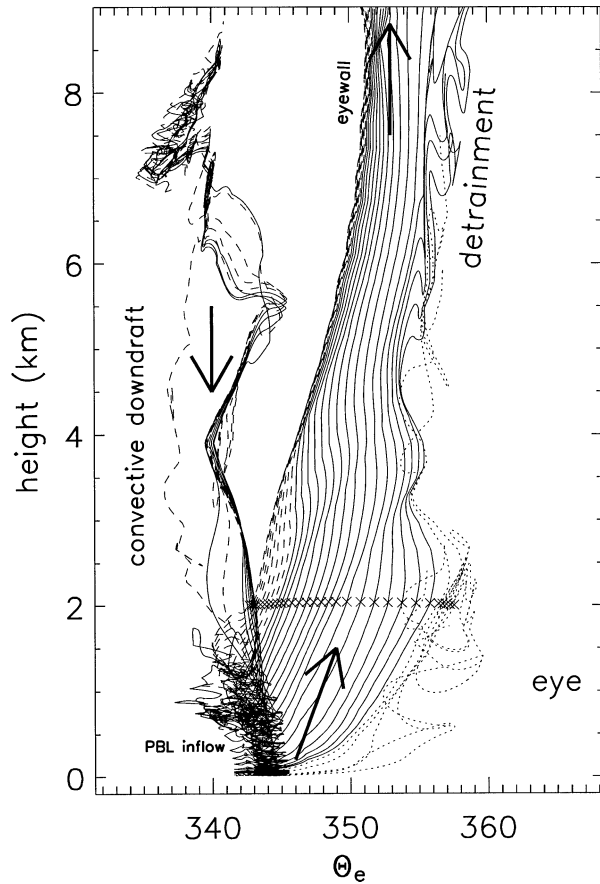


FIG. 9. The same trajectories as Fig. 8, displayed as a function of θ_e and height. Dotted trajectories enter the eyewall from the eye; solid trajectories enter the eyewall from the boundary layer inflow dashed trajectories enter the eyewall from above the boundary layer; Xs mark the seeding locations.

voir also experiences an enhanced heat sink due to its proximity to the imposed forcing, which also might in part explain the weaker storm.

6. Heat or buoyancy?

What remains is to establish the means by which the introduction of air with high entropy from the eye to the eyewall produces a stronger storm. The candidate phenomena come in two classes: those that necessarily invoke the nonhydrostatic properties of the RE87 model and those phenomena that can be well described with hydrostatic principles.

It is known that nonhydrostatic processes in tornadoes can drive wind speeds to more than twice the limit suggested by thermodynamic forcing of buoyancy in the environment of the tornado (Fiedler and Rotunno 1986; observationally confirmed by Bluestein et al. 1993). Fielder (1994) shows that this can come about through either one of two phenomena: 1) an end-wall vortex, or 2) a drowned vortex jump. An end-wall vortex has its updraft directly at the axis of rotation that does not

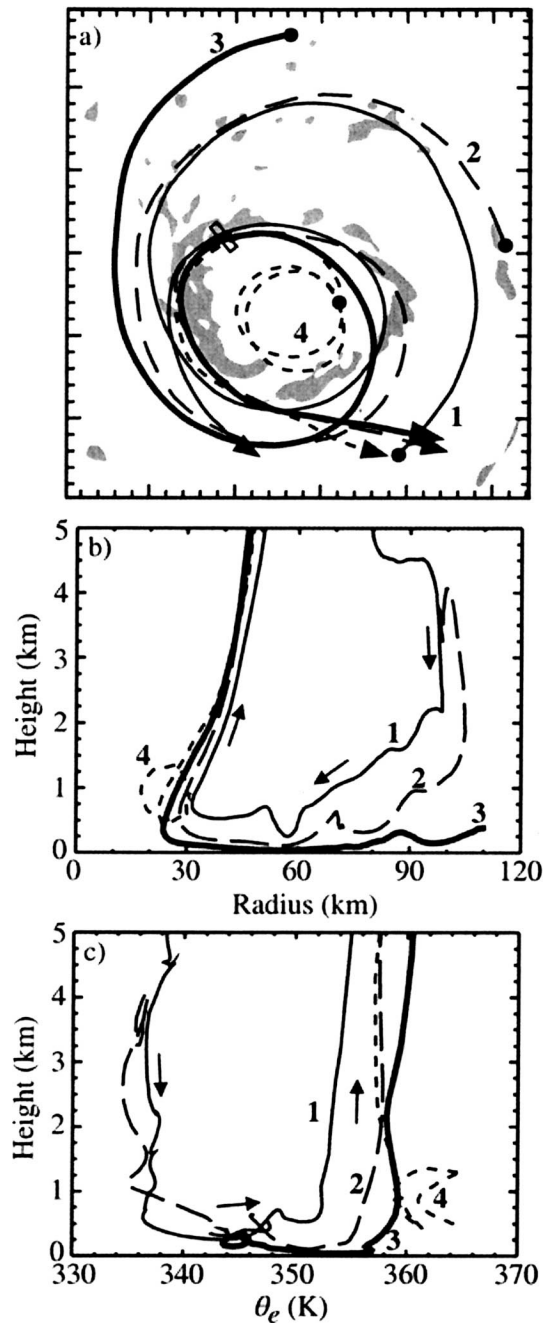


FIG. 10. Figure 13 of Braun (2002), displaying trajectories from a 3D simulation of Hurricane Bob using the MM5 model. The trajectories are seeded at a point of locally enhanced ascent within the eyewall. (a) Horizontal projection of the trajectory paths in a reference frame moving with the storm. Shading indicates simulated reflectivities greater than 40 dBZ at 66 h from initialization. Filled circles and arrowheads indicate the beginnings and ends, respectively, of the trajectories. The small rectangular box indicates where the trajectories were seeded. (b) Profiles of trajectory radius vs height. (c) Profiles of trajectory θ_e vs height. In (b) and (c), small arrows indicate the general direction of movement of the air parcels.

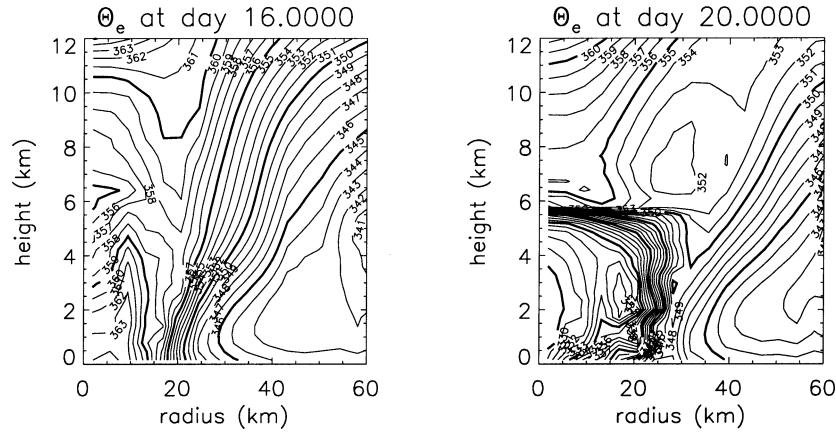


FIG. 11. Cross section of Θ_e (K) from the 4x run before and after imposition of an artificial heat sink in the lower eye.

resemble our simulated hurricane. The drowned vortex jump has its peak updraft at a nonzero radius and bears superficial similarities to a hurricane vortex. The drowned vortex jump is out of cyclostrophic balance and results from “nearly loss-free ‘overshoot’ of the radial inflow into nearly the lowest pressure of the core [of the tornado-like vortex]” (Fielder 1994). The drowned vortex jump of Fielder (1994) shows a local pressure minimum near the radius of maximum low-level winds at the point where the inflow is stopped and directed upward that is different from Fig. 1b. Figure 1b suggests that the pressure perturbation is downward-directed and in part argues against a dynamic pressure force.

Eliassen’s (1951) balanced vortex model, which assumes that the vortex evolves near a state of gradient and hydrostatic balance, can be used to further test the importance of nonhydrostatic effects in storm maintenance. The equation for the transverse streamfunction ψ under the Boussinesq approximation is given by

$$\frac{\partial}{\partial r} \left(\frac{N^2}{r} \frac{\partial \psi}{\partial r} - \frac{\xi}{r} \frac{\partial v}{\partial z^*} \frac{\partial \psi}{\partial z^*} \right) + \frac{\partial}{\partial z^*} \left(\frac{\eta \xi}{r} \frac{\partial \psi}{\partial z^*} - \frac{\xi}{r} \frac{\partial v}{\partial z^*} \frac{\partial \psi}{\partial r} \right) = \frac{\partial Q}{\partial r} - \frac{\partial}{\partial z^*} (\xi F), \quad (13)$$

where N is the Brunt–Väisälä frequency, F is the “external” (including temporal eddy) forcing term for v , $(\theta_0 Q/g)$ is the external forcing term for potential temperature θ . Here,

$$z^* = \left[1 - \left(\frac{p}{p_0} \right)^{(\gamma-1)/\gamma} \right] \frac{\gamma}{\gamma-1} \frac{p_0}{\rho_0 g} \quad (14)$$

is the pseudoheight (Hoskins and Bretherton 1972), where p_0 is a reference pressure, ρ_0 is a reference density for computing the scale height, and $\gamma = c_p/c_v$ is the ratio of the specific heats of dry air. In (13),

$$\eta = f + \frac{v}{r} + \frac{\partial v}{\partial r} \quad (15)$$

is the absolute vertical vorticity, and

$$\xi = f + \frac{2v}{r} \quad (16)$$

is the modified Coriolis parameter. From (13), the secondary circulation of an axisymmetric mean vortex evolving near a state of gradient wind and hydrostatic balance can be solved for given known momentum forcing F and heat forcing Q [Möller and Shapiro (2002) explain the methodology for regularizing the axisymmetric state in order to produce a solution; Persing et al. (2002) used this technique in their study]. Since the forcings of momentum and heat can be derived from daily averaged numerical output, our hypothesis is that, if the resulting secondary circulation from (13) agrees closely with the secondary circulation output from the model, then the phenomenon described by the model is evolving primarily in gradient wind and hydrostatic balance. Figure 12 provides such a comparison, with the inflow and updraft of the storm well-represented in structure and intensity by the Eliassen balanced vortex model. Appealing to the principle of Ockham’s razor, it is therefore believed that the model storm is evolving largely in a hydrostatic manner, and nonhydrostatic effects do not need to be invoked to explain superintensity. Some interesting differences are also evident in Fig. 12, namely in the boundary layer inflow, which penetrates to a smaller radius (18 km) in the simulation. This appears to be a boundary layer overshoot that can lead to a slight enhancement of observed tangential winds over the gradient wind (Shapiro 1983; Smith 2003).

If we appeal to the conceptualization of E-MPI as a Carnot heat engine (Emanuel 1988), then the hurricane is a mechanism for producing work by processing heat. The measure of work performed ultimately is the dissipation of the system, and the rate of dissipation in-

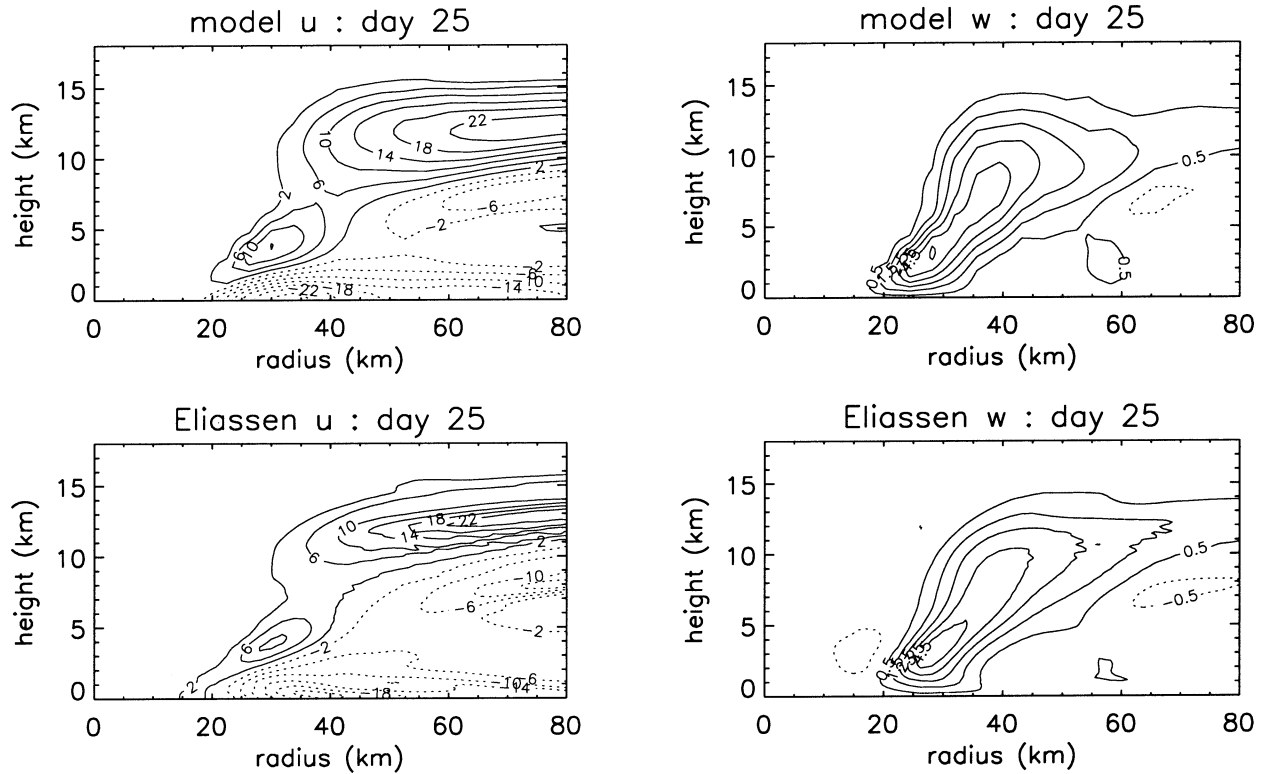


FIG. 12. The daily averaged secondary circulation observed from the 4x run at day 25, and the same inferred from the Eliassen (1951) balanced vortex model using the observed axisymmetric structure and forcings at the same time.

creases with the intensity of the storm. A stronger storm would thus require more heat addition to produce more work. The explanation of superintensity then simply comes down to added heat in the eyewall, which in part motivates the section title. Heat addition is of course not inconsistent with the generation of local buoyancy as discussed in Braun (2002) and the stretching of vortex tubes, but the distinction here is that, if the storm intensity is a function of the addition of heat (in the spirit of E-MPI theory) the role of local buoyancy is secondary or simply consistent.

E-MPI assumes that all the addition of heat to the eyewall is through its base via exchange with the ocean. The evidence presented here suggests that there is additional heat provided from an interaction with the eye. E95b (section 4, 3973–3974) explicitly noted that this assumption represents a potential weakness of maximum intensity theory. The Carnot derivation of E-MPI (Emanuel 1988) takes the boundary layer inflow as the isothermal expansion step where heat is added (see a standard physics text; e.g., Halliday and Resnick 1988); the eyewall updraft as the (moist) adiabatic expansion step; and the outflow and descent as a combined isothermal compression and adiabatic compression step.⁵ The

boundary layer inflow can then be referred to as the *warming phase* of the cycle, and the outflow and descent as the *cooling phase*, although the definition of T_{out} provided by (10) includes implicitly the eyewall as part of the cooling phase. Under the idealized assumption of moist adiabatic eyewall ascent of E-MPI theory, though, inclusion of the eyewall would not impact T_{out} . We might propose to extend the warm phase to include the eyewall where heat addition is observed to occur. In this spirit one can consider the warming of updraft parcels relative to a moist adiabat. At the top of the eyewall updraft air has had the full benefit of the eye interaction and can be compared to properties of air at the base of the eyewall as a measure of the interaction. At the top of the eyewall, q_v is much less than that found near the surface; thus, the augmentation of Θ_e is ultimately realized as changes in θ . The changes in θ , as a measure of heat addition, suggest the following ad hoc modification of SST in E-MPI to model the modified warm reservoir:

$$\text{SST}' = \text{SST} + \Delta\Theta_e = \text{SST} + (\Theta_{e,\text{out}} - \Theta_{e,\text{sfc}}), \quad (17)$$

where $\Delta\Theta_e$ mimics the heat addition from the base of the eyewall ($\Theta_{e,\text{sfc}}$) to the top ($\Theta_{e,\text{out}}$). Inspection of Figs. 9 and 16 generally shows $\Delta\Theta_e \approx 8$ K, which represents a significant augmentation of SST' from 26° to 34°C. With this modification E-MPI provides intensities of up to 80 m s⁻¹. Compared to the approximations of E-MPI summarized in the appendix that do not provide such a

⁵ While it can be argued whether real storms actually complete the cycle, examination of recirculating trajectories in the axisymmetric model here suggest that the cycle can occur in ≈ 14 days.

close estimate of the observed model intensity ($\approx 90 \text{ m s}^{-1}$), we believe that the violation of the related assumptions of vanishing heat exchange from the eye to the eyewall and moist neutral ascent are principally responsible for the observed superintensity.⁶ As E-MPI is an estimate of the magnitude of the gradient wind, one can appeal to theoretically based frictionally induced enhancements of tangential wind speed of $\approx 7\%$ found in Shapiro (1983). Alternately, one may observe that the 7 m s^{-1} underestimation of (6) by the complete E-MPI calculation (Fig. 3; dashed curve larger than the dotted curve) can be considered a measure of the error incurred in piecing the eyewall solution together with the environment. It should be noted that this modification of E-MPI is ad hoc and simply diagnostic since we do not know a priori the magnitude of the warming ($\Delta\Theta_e$) of the eyewall. An improved formulation of MPI starting from first principles to include this effect, whether as a modification of E-MPI or not, would seem to be of considerable scientific value.

7. Three-dimensional evidence for superintensity

Our explanation of superintensity in the RE87 model is that the eyewall is able to utilize of a second source of heat available from the eye. Although, in reality, E-MPI is rarely exceeded (Emanuel 2000), this mechanism may play a role in boosting the intensity of observed hurricanes that are subject to adverse conditions. Figure 13 shows results from an MM5 simulation of Hurricane Bob employing an unprecedented horizontal grid spacing of 1.3 km on the finest grid (Braun 2002; J. Fulton 2001). The mean RMW (dotted circle) at this time was 37 km and the mean radius of peak updraft (not shown) is 41 km. Equivalent potential temperature (exponential form) θ_e at the $z = 1135 \text{ m}$ level is enhanced in the eye (pink) relative to the eyewall (blue). Positive anomalies in θ_e at the edge of the θ_e enhancement (the interface between the eye and the eyewall) are on the southeast (outward advecting) side of positive invertible moist potential vorticity (PV) (IMPV; Schubert et al. 2001)⁷

⁶ If we were to extend the analogy of the Carnot engine, the addition of heat from the low-level eye could be thought of as a Carnot turbocharger, because warm eye air represents an untapped energy source just as the blow-down pressure of air exiting a normally aspirated engine represents an untapped “free” energy source that can be used to power an air pump [i.e., a turbocharger; see a standard text such as Heisler (1995) for more details on automotive engines]. The proposed impact of dissipational heating (Bister and Emanuel 1998; Businger and Businger 2001) can analogously be interpreted as a Carnot supercharger, because the energy for a supercharger is extracted directly from the useful work of the engine while dissipational heating is extracted directly from the kinetic energy field of the storm.

⁷ See Fulton (2001) for a comparison of dry PV and IMPV. Dry PV is found to be largely similar to IMPV, which includes the thermodynamic properties of dry air and water vapor plus the liquid and ice mass. Use of θ_e as the thermodynamic variable to compute PV (“moist PV”) is, of course, quite different and generally noninvertible (McIntyre 1992; Schubert et al. 2001).

anomalies. Fulton (2001) provides anecdotal evidence that, when these θ_e anomalies encounter the eyewall, they are associated with localized enhancements in updraft speed. Braun (2002) shows quantitatively that these vortical “hot towers” carry the majority of the updraft mass flux of the eyewall. Braun (2002) has further shown that these vortical hot towers are associated in this simulation of Hurricane Bob with the end points of a wavenumber-2 asymmetry that has an angular velocity that is well described by that of a barotropic vortex Rossby wave. There is an obvious suggestion then for a possible local generation of buoyancy, but Braun (2002) also shows that, in contrast to Zhang et al. (2000), a dynamic pressure force does not drive hot tower ascent above the approximate inflow boundary layer. Zhang et al. (2002) show supporting evidence of this in an MM5 simulation of Hurricane Andrew (1992) with a pronounced maximum of θ_e (to 391 K) in the low-level eye.

Frank and Ritchie (2001, their Fig. 16) present another MM5 simulation with peak tangential wind speeds greater than 100 m s^{-1} for a simulated hurricane over 28.5°C SST for a case of low vertical shear. E-MPI, assuming $\mathcal{H} = 80\%$ and reasonable range of outflow temperatures (-65° to -75°C), would be between 63 and 68 m s^{-1} (see Fig. 2). Thus, E-MPI is exceeded significantly for this three-dimensional simulation. Frank and Ritchie (2001, their Fig. 7b) also show a low-level enhancement of θ_e in the eye, but did not recognize this as a superintense situation because they used minimum central pressure as the E-MPI metric rather than maximum tangential winds. As far as the derivation of E-MPI (E95b) is concerned, recall that V_{\max} is obtained first for a given thermodynamic environment. Central pressure is obtained next with further assumptions and approximations given V_{\max} . We believe V_{\max} is the more robust metric of E-MPI, and suggest that Frank and Ritchie (2001) show at least one three-dimensional superintense hurricane simulation.

Willoughby (1998) provides independent observational evidence that the low-level eye at times (Fig. 14) may have higher entropy air than the eyewall (by more than 10 K). From Willoughby (1998) we can also infer that aircraft flight-level data is not always indicative of the low-level eye entropy structure, depending on the altitude of the inversion level (Kossin and Eastin 2001). The boundary layer in our RE87 model is given 20 days to respond (Fig. 15) to the intensity and surface fluxes of the hurricane, while real hurricanes are hardly allowed to attain a steady state for a period of many days. To illustrate this point the model eye sounding does not show a sharp inversion and Θ_e is minimized at midlevels (400 mb) rather than remaining constant with height as observations show (e.g., Willoughby 1998). After constructing a composite of dropsonde data obtained from the National Oceanic and Atmospheric Administration (NOAA) P-3 aircraft, LeeJoice (2000) finds that eye soundings at $0 \leq z < 3000 \text{ m}$ average 5 to 10 K warmer

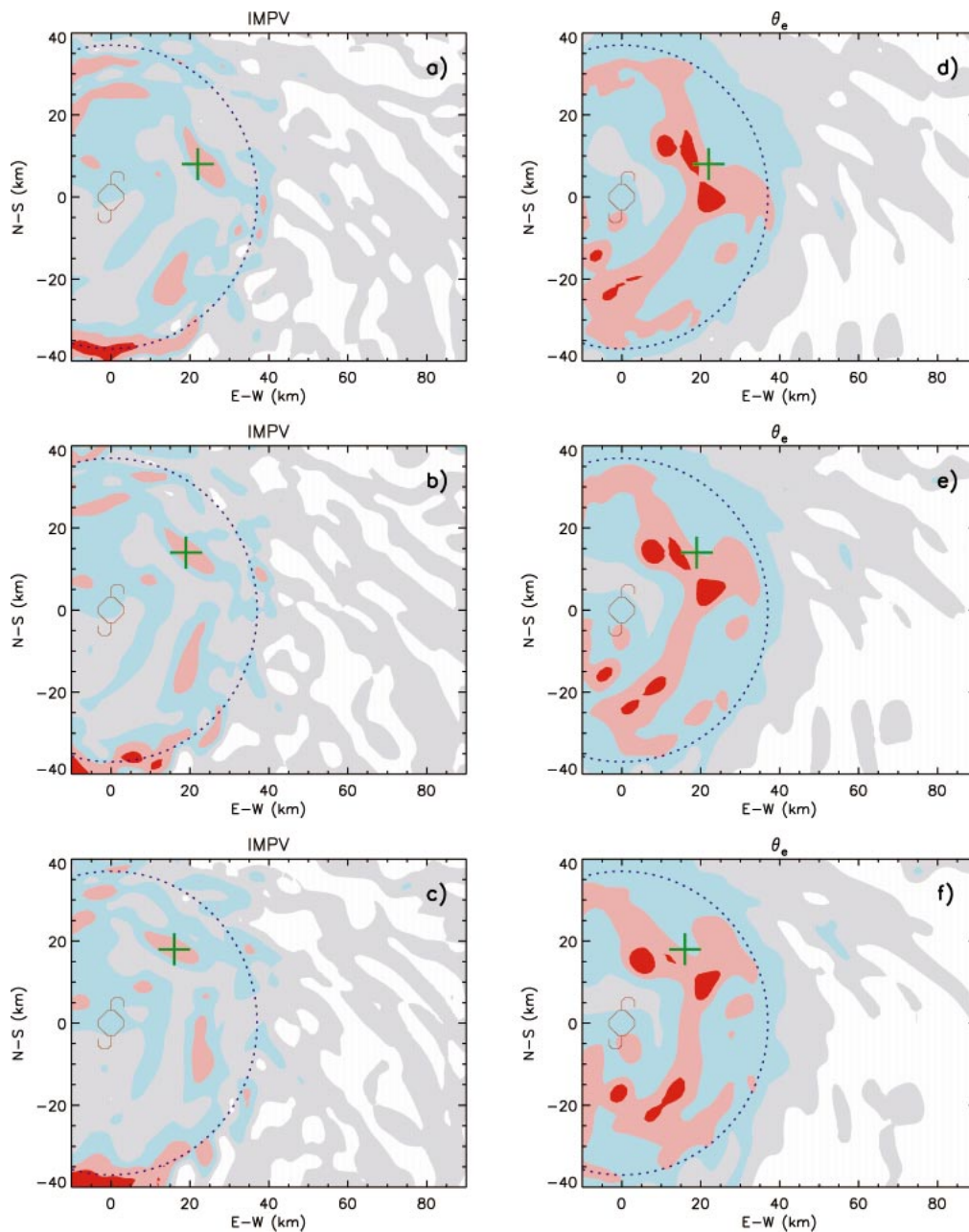


FIG. 13. IMPV at $z = 1135$ m at (a) 268, (b) 272, and (c) 276 min into an MM5 simulation of Hurricane Bob, kindly provided by S. A. Braun, NASA/GSFC (see Braun 2002 for details). Data is reported at the 1.3-km grid spacing of the innermost mesh. (d)–(f) Equivalent potential temperature θ_e displayed at respective times. The hurricane symbol denotes the storm center. Levels of shading in (a)–(c) denote no shading: $\text{IMPV} < 0$ PVUs; grey shading: $0 < \text{IMPV} < 15$ PVUs; blue shading: $15 < \text{IMPV} < 30$ PVUs; pink shading: $30 < \text{IMPV} < 60$ PVUs; red shading: $\text{IMPV} > 60$ PVUs. Levels of shading in (d)–(f) denote no shading: $\theta_e < 345$ K; grey shading: $345 < \theta_e < 351$ K; blue shading: $351 < \theta_e < 357$ K; pink shading: $357 < \theta_e < 363$ K; red shading: $\theta_e > 363$ K. The dotted circle is the radius of maximum winds, $r = 37$ km. The “+” is to mark the position of a typical enhancement of IMPV interior to the RMW. Cyclonic motion around this IMPV enhancement appears to position high- θ_e air radially outward to the RMW around the southeast side of the feature. Figure adapted from Fulton (2001).

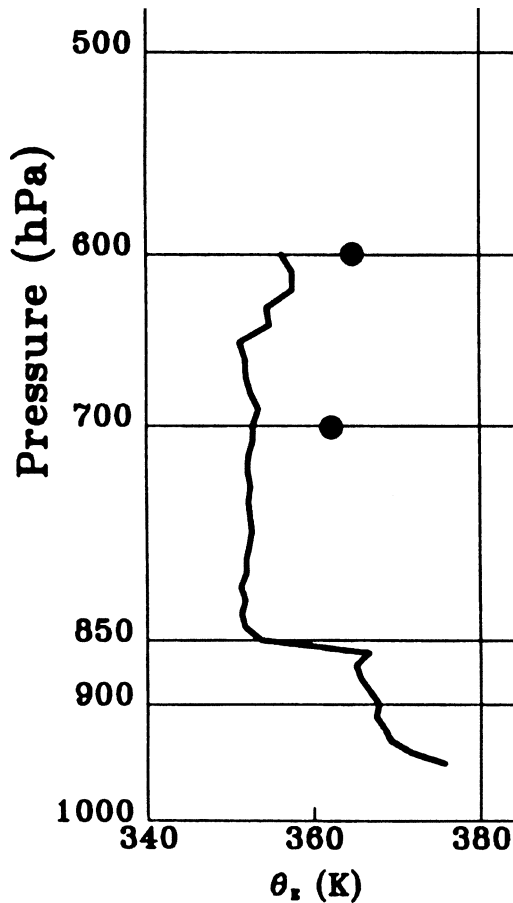


FIG. 14. Dropsonde retrieval of θ_e (solid curve) from the eye of Hurricane Jimena (eastern Pacific, 2058 UTC 23 Sep 1991) compared to θ_e measured on board aircraft at the moment of eye penetration (large dots), defined by the last measurement of saturation. Figure adapted with kind permission from Willoughby (1998).

(in terms of θ_e) than in the eyewall. This attribute is confirmed in the RE87 model in Fig. 15. LeeJoice (2000) also finds that dropsondes show little vertical gradient in terms of θ_e in the eyewall, but a significant gradient (10 K over 3000 m) in the eye, generally supporting our interpretation of Willoughby (1998) and the observed moist entropy structure in our simulations.

8. Discussion

We have demonstrated that the RE87 model will produce a model storm of increasing intensity with increasing resolution. Convergence in the maximum tangential winds was found with sufficiently high resolution. Hausman (2001) suggested that the increase in storm intensity is due to decreases in the RMW at higher resolution; smaller RMWs simply were not resolvable at coarse resolution. Our finding with the RE87 model is that the RMW stabilizes by the 2x run, but increases in intensity further occur to the 4x run (Table 2). Because E-MPI has been presented previously as a rigorous upper bound

on hurricane intensity, an investigation into its theoretical bases was warranted. E-MPI theory provides the context for extracting and summarizing the key phenomena for superintensity.

Figure 16 summarizes many of the important interactions associated with the superintensity phenomenon, where the abscissa is displayed as a function of absolute angular momentum ($M = rv + fr^2/2$). We have demonstrated a low-level entropy maximum in the eye (Fig. 16, Θ_e contours in red) that is associated with superintensity relative to E-MPI and an interaction between the warm eye and the eyewall (Fig. 16, blue streamlines near $M = 1 \times 10^6 \text{ m}^2 \text{ s}^{-1}$). After showing that the storm evolves largely in gradient and hydrostatic balance, the related assumptions of E-MPI theory that the eyewall is in slantwise, moist adiabatic ascent without interaction with the eye are violated (Fig. 16, noting from the vertical alignment of streamlines in the green shaded, saturated eyewall region of the storm that angular momentum is better conserved than Θ_e). Through a simple addition of heat much of the superintensity of the modeled storm can be explained with an ad hoc modification of E-MPI.

The eddy features in the streamlines of Fig. 16 can be recognized as the breakdown of an azimuthal vortex sheet and as a primary advecting mechanism for high-entropy air between the eye and the eyewall. With a vertical scale of only about 1 km, these features are not resolvable at low vertical resolution. Associated with these eddy features is a tangential vorticity of $\approx -1 \times 10^{-2} \text{ s}^{-1}$ (not shown). A low-level outflow jet is identifiable, perhaps, below $z < 1 \text{ km}$; however, the eddies extending up to $z = 5 \text{ km}$ are distinct from the low-level jet.

The internal redistribution of heat within the eyewall by diffusion raises the question whether the basic result presented here is a peculiarity of the diffusion scheme of the model. An experiment at 4x resolution using a greatly reduced diffusion (by a factor of 16 from the 4x run, mixing length l_h by a factor of 4; see Table 3) suggests that the role of diffusion is replaced by temporal eddies, and the time series of V_{\max} (not shown) exhibits a shorter period variability of $\approx \pm 4 \text{ m s}^{-1}$ from the long-term mean, but still is superintense ($V_{\max} \approx 85 \text{ m s}^{-1}$). Although the energetic inconsistency of the RE87 model is a potential issue (K. Emanuel 2002, personal communication), the fact that superintensity persists as the mixing length is decreased substantially suggests that the subgrid-scale effects are not the reason for the superintensity phenomenon. Moreover, the availability of at least one source of high entropy (the ocean beneath the eye) and the resolved-scale breakdown of a transverse vortex sheet argue that some aspect of this superintensity mechanism should still operate in a variety of real situations.

A mathematical proof is not known to the authors of whether a nonlinear dynamical system prefers to exist in a state that maximizes the rate of entropy production,

Soundings from 4x Run at day 20

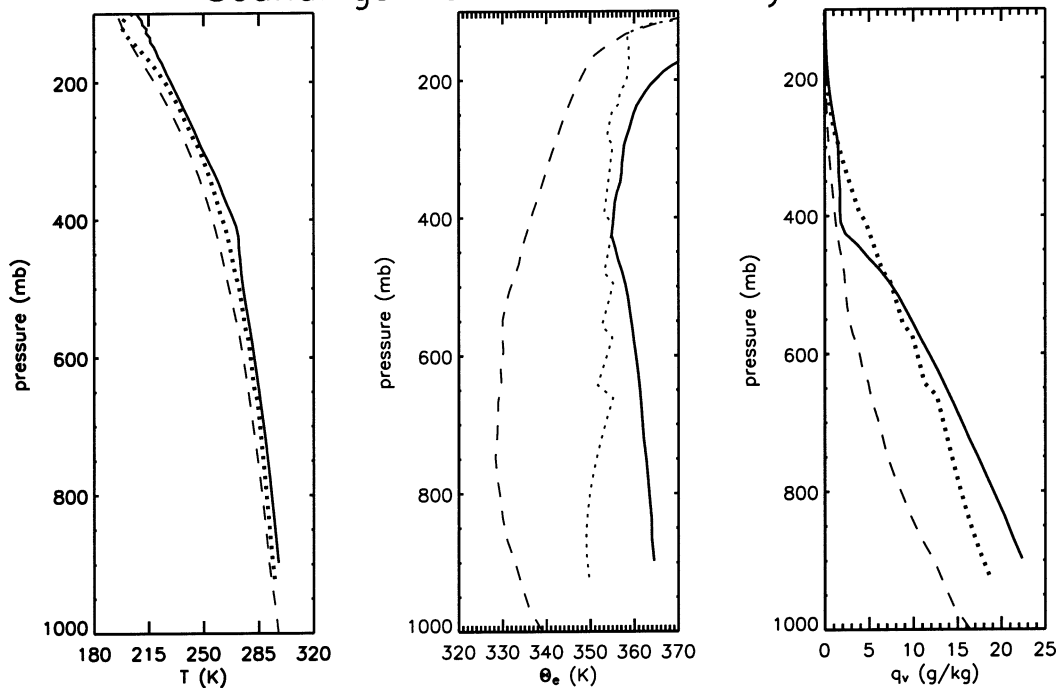


FIG. 15. Soundings for the eye (solid; computed at $r = 0$ km), the eyewall (dotted; computed at the radius of peak updraft), and the environment (dashed; averaged over $r > 800$ km). The eyewall sounding shows jaggedness because of the discrete outward jumps in radial grid steps of the peak updraft.

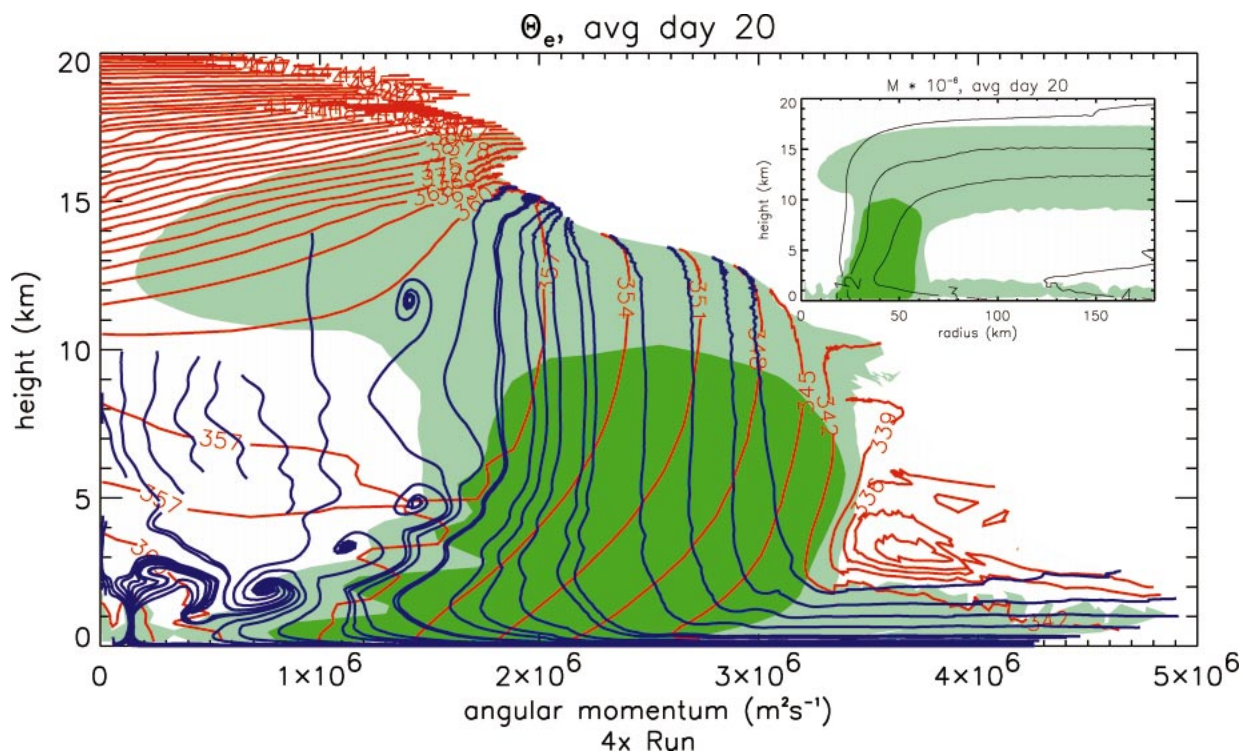


FIG. 16. Equivalent potential temperature Θ_e (K; red, 1-day average) displayed as a function of absolute angular momentum and height at day 20 in the 4x run. Overlaid are 2D streamlines of the daily averaged secondary circulation (blue). Light green shading denotes $q_1 > 0.3 \text{ g kg}^{-1}$. Dark green shading denotes $q_1 > 1 \text{ g kg}^{-1}$. The inset figure repeats the shading for q_1 , displayed as a function of physical radius. The contours of absolute angular momentum (black, inset) are provided for physical reference for the main figure.

TABLE 3. Comparison of modeled intensities using the RE87 model. (BE98 refers to Bister and Emanuel 1998; CAPE is convective available potential energy.)

Experiment	Resolution		Approx $\langle V_{\max} \rangle$ (m s ⁻¹)
	Radial	Vertical	
RE87 control unbounded radiative cooling	1x	1x	46
RE87 experiment J (radiative cooling ≤ 2 K day ⁻¹)	1x	1x	51
BE98 no dissipational heating	2x	1x	67
BE98 dissipational heating	2x	1x	80
1x run before day 15	1x	1x	55
1x run after day 15	1x	1x	62
2x run	2x	2x	80
4x run	4x	4x	90
4x run ($I_e \times 4$ relative to 4x run)	4x	4x	65
4x run ($I_e/4$ and $I/4$ relative to 4x run)	4x	4x	85
4x run (SST = 28°C; equilibrated sounding)	4x	4x	102
4x run (SST = 28°C; Jordan sounding)	4x	4x	105

but Sawada (1981) provides a compelling argument for such a system bounded by two infinite thermal reservoirs. Under different conditions, different dynamical pathways are simply not available, which was used to describe, for example, different crystallization habits or convection modes between plates as states where pathways become available as geometric or thermodynamic constraints are relaxed. Different physical systems have been demonstrated to exist in or relax toward states of maximum entropy or maximum rate of entropy production (e.g., Malkus and Veronis 1958; Malkus and Riehl 1960; Stephens and O'Brien 1993; O'Brien 1997; Ozawa and Ohmura 1997; Jin and Dubin 1998; Schubert et al. 1999; Schechter et al. 1999; Paltridge 2001; Lorenz et al. 2001). The superintense behavior of the RE87 model at high resolutions may simply be the heat engine existing in a more effective dynamical pathway. What remains as future work is to explain why superintense behavior of hurricane models is a preferred pathway and to discover the constraints on accessing this pathway.

Sensitivity studies with the horizontal subgrid-scale parameterization in the RE87 model (not shown) indicate that a more diffusive simulation will produce a weaker (yet still superintense) storm. Since the eyewall warming ($\Delta\Theta_e$) observed in these experiments is likewise reduced, we believe the picture presented here is still consistent. Diffusion in the axisymmetric model not only models the effect of subgrid-scale axisymmetric mixing, but more prominently serves as a crude surrogate for the impact of otherwise resolvable asymmetries. Barotropic instability (Michalke and Timme 1967; Schubert et al. 1999) naturally results from a ring of convection (an ideal eyewall) due to vortex tube stretching, which would lead to the growth of vortex Rossby waves and eventually nonlinear, coherent vortex structures (eyewall mesovortices; Kossin and Schubert 2001; Montgomery et al. 2002). The radial structure of axisymmetric mean vorticity in a steady-state three-dimensional storm should be an approximate balance between sources due to convection and losses due to redistribution and friction. In a similar manner, the low-

level entropy reservoir is a balance between an ocean source and loss to the eyewall (and to a lesser extent radiation). In a steady-state view, a slower mixing rate (less vigorous vortex Rossby waves and mesovortices) allows the entropy reservoir to build to greater levels and potentially allow for more eyewall warming ($\Delta\Theta_e$). In a more realistic, time-varying hurricane, the existence of more vigorous mixing may promote short-term intensification of the vortex and a temporary exhaustion of the heat reservoir. What remains as a basic question for future research is the role of vortex Rossby waves and eyewall mesovortices (Montgomery et al. 2002) in mixing thermodynamic properties and their impact on MPI.

Many mechanisms have been proposed that would provide a storm intensity that would be weaker than E-MPI. Adverse vertical wind shear is believed to disrupt the thermal maximum of the upper-level eye, providing for a weaker central pressure (Gray 1968; DeMaria 1996; Frank and Ritchie 1999, 2001). Secondary eyewalls are found in very intense hurricanes (Willoughby et al. 1982) that interrupt the radial inflow of environmental angular momentum (Camp and Montgomery 2001); intensity fluctuations are found with eyewall replacement cycles. Hausman (2001) found that axisymmetric hurricane simulations using ice microphysics are weaker than comparable rain-only simulations. De-Cosmo et al. (1996) suggest that the ratio of C_k/C_D becomes less than unity at high wind speeds, although Andreas and Emanuel (2001) present an argument that an accounting of the entropy flux due to reentrant sea spray could lead to a positive flux of entropy that nearly cancels the anticipated reduction of V_{\max} from changes in C_k/C_D . Drag with the ocean surface generates mixing currents in the ocean that bring cool, deep ocean water to the surface, thus decreasing the effective surface temperature that the hurricane is in contact with (Shay et al. 1998; Bender and Ginis 2000; Jacob et al. 2000). In the face of these negative influences on intensity, the hurricane may take advantage of dissipational heating of the boundary layer (Bister and Emanuel 1998; Bus-

inger and Businger 2001) as a secondary heat source for the storm. Bister and Emanuel (1998) ran a version of the RE87 model that includes dissipational heating as a forcing term. This showed a 13 m s^{-1} increase in intensity with the inclusion of dissipation heating (Table 3). This compares to the 35 m s^{-1} increase associated with the eye entropy reservoir demonstrated here. Thus, eyewall heating may be as important or more important to storm intensity as dissipational heating.

9. Conclusions

While E-MPI has been previously presented as a rigorous upper bound on storm intensity, at high spatial and temporal resolution the RE87 hurricane model produces storms that greatly exceed E-MPI. Because the superintense state is well captured by Eliassen's (1951) balanced vortex model, nonhydrostatic processes on the vortex scale are not viable candidates for explaining superintensity. The cause of superintensity is found to lie in the presence of high-entropy air in the low-level eye, which is entrained into the eyewall. The introduction of high-entropy air from the eye represents an additional source of heat to the eyewall of the storm and leads to a modified Carnot cycle that supports a stronger storm. Observational evidence points to the existence of this mechanism in real hurricanes and also in three-dimensional numerical models.

It is proposed that a new MPI should be formulated from first principles that incorporates this effect, whether as a novel approach to the problem or as a modification of E-MPI. It is proposed that further analyses of the thermodynamic structure of both idealized and real-case simulations of hurricanes be conducted in three dimensions. An interesting outcome of this work that bears further scrutiny is that the axisymmetric hypercane regime described by Emanuel (1988) may become more accessible with small perturbations of presently observed thermodynamic characteristics of the atmosphere (Knutson and Tuleya 1999). Whether hypercanes are indeed even possible in a three-dimensional context is an open question that will be the consideration of upcoming work.

Acknowledgments. This work was supported in part by Office of Naval Research Grants N00014-93-1-0456 P00006, N00014-02-1-0474, National Science Foundation ATM-0101781, National Aeronautics and Space Administration (NASA) Fourth Convective and Moisture Experiment (CAMEX) Grant NAG5-11140, and Colorado State University. We would like to thank R. Rotunno for kindly making his model available to us and for valuable discussion that helped clarify thought and presentation. Thanks also to H. Willoughby at National Oceanic and Atmospheric Administration Atlantic Oceanic and Meteorological Laboratory's Hurricane Research Division and S. Braun of NASA Goddard Space Flight Center for the use of their figures. We

would also like to thank W. Gray, W. Schubert, K. Emanuel, M. Eastin, S. Grandlienard, T. Cram, S. Hausman, M. Kirby, G. Stephens, and D. O'Brien, and reviewers J. Kossin and S. Gray for their helpful suggestions and input.

APPENDIX

An Assessment of the Assumptions and Approximations of E-MPI

This appendix discusses some sensitivities and approximations in E-MPI that can potentially impact the estimate of intensity. We find that all of the candidate sensitivities are too small to explain the superintensity shown in high-resolution simulations of the RE87 model (see Fig. 3).

a. Balance of entropy and angular momentum

The accuracy of the combined balance of entropy and angular momentum that is central to E-MPI can be tested by comparing the left- and right-hand sides of Eq. (11) of E95b (in nondimensional terms):

$$\frac{1}{2\bar{R}}(\bar{R}^2 - \bar{r}_b^2) \frac{\partial \bar{\chi}_b}{\partial \bar{R}} = -\frac{C_k}{C_D}(\bar{\chi}_s^* - \bar{\chi}_b), \quad (\text{A1})$$

where R is the potential radius. Each term is within 30% in magnitude of the other in the vicinity of the eyewall, where the vertical difference term (rhs) is generally of less magnitude because of saturation at the eyewall of the first grid level. The derivation at this point proceeds to (6), and the square root is thus taken of the 30% error to estimate the error in V_{\max} .

b. Relative humidity

Noted in section 3b, (6) does not satisfy the requirements of an MPI theory since χ_s^* and χ_b cannot be known prior to formation of the storm. E95b invokes a closure assumption that \mathcal{H} at the eyewall can be known. For this, E95b needs to assume two things. First, that \mathcal{H} has the same value at the eyewall as in the environment; this assumption permits E95b to derive an expression for central pressure and RMW. Second, and more relevant to the estimation of V_{\max} , is that χ_b and χ_s^* can be approximately related to each other by Eq. (15) of E95b (here in dimensional form):

$$\chi_b = \mathcal{H}(\chi_s^* - \chi_{si}^*). \quad (\text{A2})$$

Implicitly, this equation again makes the first approximation that \mathcal{H} has the same value at the eyewall and the environment, but (A2) is admittedly approximate (E95b). The relative error incurred by invoking approximation (A2) to estimate χ_b is about $(1 - \mathcal{H})$, or 20% error at 80% relative humidity. One can track the error through the V_{\max} derivation by augmenting χ_b with a multiplicative constant α with a value near unity [i.e.,

$\alpha = 1 \pm (1 - \mathcal{H})$. The modification of (2) appears inside the factor γ^* (4), giving

$$\gamma^* = A \frac{1 - \mathcal{H}\alpha}{1 - \mathcal{H}A}. \quad (\text{A3})$$

The relative error in the estimate of V_{\max}^2 is much smaller (4% for $\alpha = 0.8$); for V_{\max} , it is smaller still (typical error of 1 m s^{-1} for a 57 m s^{-1} E-MPI and $\alpha = 0.8$.) The impact of having radial structure in \mathcal{H} is explicitly ignored in (A2).

Another difficulty with applying \mathcal{H} to the numerical model data is that this value strictly speaking does not exist in the RE87 model. What exists in the model is a value of q_v at grid levels with $z > 0$, and thus relative humidity at the first grid level (generally found to be saturated at the eyewall) and an assumption of exchange with a saturated surface layer in contact with the ocean. In this case, \mathcal{H} should then be thought of as the relative humidity just above the surface layer, on the order of several meters. This is just a conceptualization which the bulk aerodynamic formula may or may not recognize. Proceeding with this conceptualization and accepting the observation that the first grid level under the eyewall is saturated, then as the numerical resolution is increased, the saturated first grid level approaches the sea surface. If a well-mixed boundary layer is assumed, the value of \mathcal{H} would become more saturated, which would provide for a slower estimate of V_{\max} using (2), which is contrary to the observed behavior of the model with increasing resolution. For all of these reasons, use of (6) is believed more robust for the purpose of comparing with model output, rather than (2).

c. Boundary layer height

According to Emanuel (1995a), the top of the boundary layer is the proper reference for evaluating χ_b . In this paper, when χ_b has been evaluated, it has been at the first grid level, the level of saturation at the eyewall. At low resolution (the default run), this level ($z = 625 \text{ m}$) is also saturated in the near environment of the eyewall extending to $r \sim 80 \text{ km}$, except where downdrafts are occurring. As resolution is increased, the level of saturation in the near environment is generally found at $z = 400 \text{ m}$. Selecting this level in computation of χ_b leads to only a small increase in estimating V_{\max} using (6) at higher resolutions (4x and 8x runs) of 5 to 10 m s^{-1} , which is insufficient to explain the observed degree of superintensity.

d. Gradient wind balance

While the sensitivity of E-MPI to violation of the gradient wind approximation is difficult to track through the theory, we can test the degree to which these model runs conform to gradient wind balance

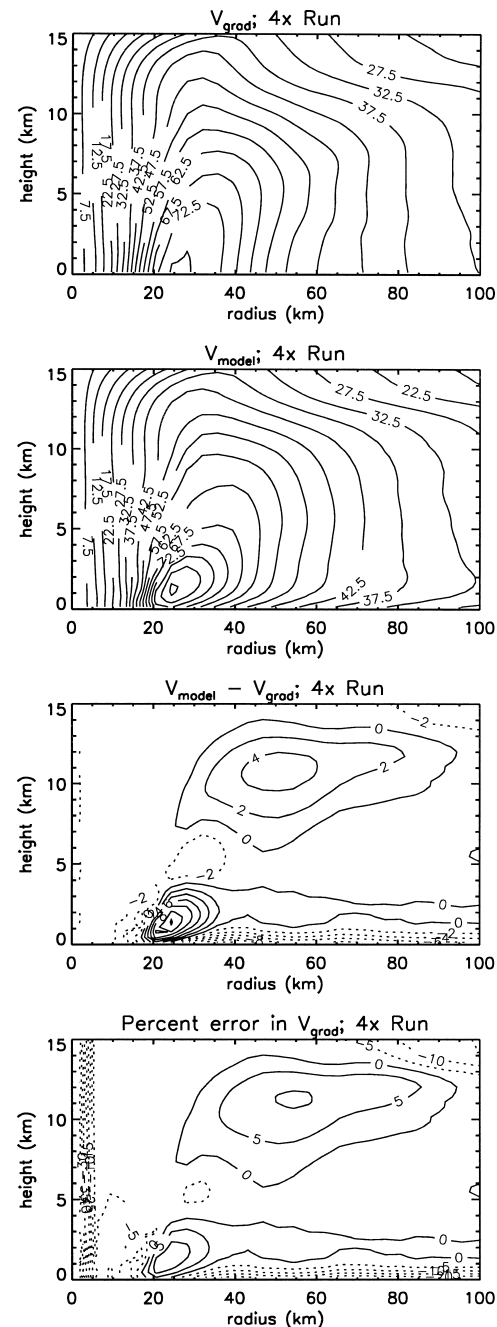


FIG. A1. The gradient wind, the model tangential wind, the difference between the two (m s^{-1}), and the relative error (%) averaged from the last 15 days of the 4x run.

$$V_{\text{gradient}} = -\frac{fr}{2} + \left(\frac{f^2 r^2}{4} + \frac{r}{\rho} \frac{\partial p}{\partial r} \right)^{1/2} \quad (\text{A4})$$

by computing the relative error

$$\frac{V_{\text{model}} - V_{\text{gradient}}}{V_{\text{model}}} \quad (\text{A5})$$

from the model output (Fig. A1). Model tangential

winds are slow in the planetary boundary layer by about 15% and too strong in the updraft by the same amount. Deceleration of the winds in the boundary layer can be anticipated from local force balance considerations. Willoughby (1990) shows a slight tendency for supergradient winds at flight-level (850 mb) of more intense storms. Elsewhere, Willoughby (1990) found that flight-level winds show no bias relative to gradient winds in many storms. The gradient imbalances are approximately the same in the default run and the 4x run and therefore gradient wind imbalance cannot be invoked to explain the emergence of superintensity at higher resolution. Further, these results are in general agreement with a small degree of supergradient winds found in Shapiro (1983, his section 2). See section 8 for more.

e. Thermal wind balance

One intriguing aspect of the E95b derivation of E-MPI is the origin of the “thermal wind” equation valid at the top of the boundary layer (and by the moist neutral assumption, through all the troposphere except the boundary layer) repeated here as in E95b in nondimensional form (using tildes to denote nondimensional quantities):

$$\frac{1}{\tilde{r}_b^2} = -\frac{2}{\tilde{R}^3} \frac{\partial \tilde{\chi}_b^*}{\partial \tilde{R}}. \quad (\text{A6})$$

At one point in Emanuel’s derivation of V_{\max} it becomes necessary to assume that the eyewall and the near environment are neutral to moist ascent along surfaces of constant absolute angular momentum M , and that rising parcels travel along such M surfaces. A consequence of this assumption is that the moist entropy is constant on M surfaces. If the atmosphere in this area is under persistent saturated ascent, as in a hurricane, then saturated entropy s^* is also constant on M surfaces above the boundary layer (assumed to be the same as the lifted condensation level). Because of this, the thermal structure of the atmosphere can simply be described as a function of M , which is the key to interpreting (A6) as a thermal wind relationship. Under these assumptions, the derivative $\partial s^*/\partial M)_p$ is a simple function of M and is independent of height because s^* has a one-to-one relationship to M . An integral dp along M surfaces is then performed to collapse the vertical structure of the atmosphere and to describe the troposphere in terms of quantities at the top of the boundary layer, a guiding philosophy of E-MPI. Under the moist neutral assumption, $\partial s^*/\partial M$ is then simply a constant that comes out of the integral.

We can relax the moist neutral assumption in one specific way such that (A6) would still be valid (subject to other assumptions of the derivation like gradient wind balance; hydrostatic balance; and persistent, slantwise convection, for example). Specifically we can relax the assumption that $\partial s^*/\partial M)_p$ is a constant along M surfaces, which would permit some moist static stability so long

as that stabilization has more or less the same vertical structure on different M surfaces.

Relaxing the assumption that $\partial s^*/\partial M)_p$ is constant along M surfaces, the problem then becomes, to what degree does

$$\left. \frac{\partial s_b^*}{\partial M} \right)_p \quad (\text{A7})$$

approximate the average

$$\left\langle \frac{\partial s^*}{\partial M} \right\rangle_p \equiv \frac{1}{p_{\text{out}} - p_b} \int_{p_b}^{p_{\text{out}}} \left. \frac{\partial s^*}{\partial M} \right)_p dp \quad (\text{A8})$$

using path integrals along an M surface to define a tropospheric average? Estimating the error in using (A7) with a multiplicative factor α_1 (where $\alpha_1 = 1$ would imply no error) allows (A8) to be rewritten as

$$\left\langle \frac{\partial s^*}{\partial M} \right\rangle_p = \alpha_1 \left. \frac{\partial s_b^*}{\partial M} \right)_p, \quad (\text{A9})$$

where brackets denote the average defined above. This error then modifies the thermal wind relation (A6) as follows:

$$\frac{1}{\tilde{r}_b^2} = \frac{-2\alpha_1}{\tilde{R}^3} \frac{\partial \tilde{\chi}_b^*}{\partial \tilde{R}}, \quad (\text{A10})$$

which can be carried through to modify the boundary layer balance estimate of V_{\max} (6) to become

$$V_{\max}^2 = \alpha_1 \frac{C_k}{C_D} (\chi_s^* - \chi_b). \quad (\text{A11})$$

Because of the square root dependence of V_{\max} on α_1 , the dependence of V_{\max} on the magnitude of this error then becomes significantly reduced. Motivated by the presence of a low-level entropy enhancement (like Fig. 16, where Θ_e^* strongly tracks Θ_e) that visibly distorts the radial gradient of saturated entropy above that found at PBL top, the value of α_1 was tested. For the many cases evaluated, generally $1 \leq \alpha_1 \leq 1.1$.

Thus, although the approximations used in deriving (A6) can be somewhat relaxed using values found in our model runs, they are incapable of explaining superintensity.

f. Outflow temperature

From (A8), it is clear that the meaning of T_{out} should be at the end point of the integral defined above. This would appear to permit different values of T_{out} as a function of radius. Also T_{out} would be defined at a point, rather than as an average as defined by (10), and would be generally colder than (10). There is no reason to anticipate that this definition of T_{out} would be greatly different than that defined by (11), used elsewhere in this paper. In any case, no reasonable value of T_{out} supplied into E-MPI theory can explain the degree of superintensity observed in our model runs.

REFERENCES

- AMS Council, 2000: Policy statement: Hurricane research and forecasting. *Bull. Amer. Meteor. Soc.*, **81**, 1341–1346.
- Andreas, E. L., and K. A. Emanuel, 2001: Effects of sea spray on tropical cyclone intensity. *J. Atmos. Sci.*, **58**, 3741–3751.
- Bender, M. A., and I. Ginis, 2000: Real-case simulations of hurricane–ocean interaction using a high-resolution coupled model: Effects on hurricane intensity. *Mon. Wea. Rev.*, **128**, 917–946.
- Bengtsson, L., 2001: Hurricane threats. *Science*, **293**, 440–441.
- Bister, M., and K. A. Emanuel, 1998: Dissipative heating and hurricane intensity. *Meteor. Atmos. Phys.*, **65**, 233–240.
- Bluestein, H. B., J. G. Ladue, H. Stein, D. Speheger, and W. P. Unruh, 1993: Doppler radar wind spectra of supercell tornadoes. *Mon. Wea. Rev.*, **121**, 2200–2221.
- Bolton, D., 1980: The computation of equivalent potential temperature. *Mon. Wea. Rev.*, **108**, 1046–1053.
- Bosart, L. F., C. S. Velden, W. E. Bracken, J. Molinari, and P. G. Black, 2000: Environmental influences on the rapid intensification of Hurricane Opal (1995) over the Gulf of Mexico. *Mon. Wea. Rev.*, **128**, 322–352.
- Braun, S. A., 2002: A cloud-resolving simulation of Hurricane Bob (1991): Storm structure and eyewall buoyancy. *Mon. Wea. Rev.*, **130**, 1573–1592.
- Businger, S., and J. A. Businger, 2001: Viscous dissipation of turbulent kinetic energy in storms. *J. Atmos. Sci.*, **58**, 3793–3796.
- Camp, J. P., 1999: Hurricane maximum intensity: Past and present. M.S. thesis, Colorado State University, 147 pp.
- , and M. T. Montgomery, 2001: Hurricane maximum intensity: Past and present. *Mon. Wea. Rev.*, **129**, 1704–1717.
- Chen, Y., and M. K. Yau, 2001: Spiral bands in a simulated hurricane. Part I: Vortex Rossby wave verification. *J. Atmos. Sci.*, **58**, 2128–2145.
- DeCosmo, J., K. B. Katsaros, S. D. Smith, R. J. Anderson, W. A. Oost, K. Bumke, and H. Chadwick, 1996: Air–sea exchange of water vapor and sensible heat: The Humidity Exchange Over the Sea (HEXOS) results. *J. Geophys. Res.*, **101**, 12 001–12 016.
- DeMaria, M., 1996: The effect of vertical shear on tropical cyclone intensity change. *J. Atmos. Sci.*, **53**, 2076–2087.
- Eliassen, A., 1951: Slow thermally or frictionally controlled meridional circulation in a circular vortex. *Astrophys. Norv.*, **5**, 19–60.
- Emanuel, K. A., 1986: An air–sea interaction theory for tropical cyclones. Part I: Steady-state maintenance. *J. Atmos. Sci.*, **43**, 585–604.
- , 1988: The maximum intensity of hurricanes. *J. Atmos. Sci.*, **45**, 1143–1155.
- , 1989: The finite-amplitude nature of tropical cyclogenesis. *J. Atmos. Sci.*, **46**, 3431–3456.
- , 1995a: The behavior of a simple hurricane model using a convective scheme based on subcloud-layer entropy equilibrium. *J. Atmos. Sci.*, **52**, 3960–3968.
- , 1995b: Sensitivity of tropical cyclones to surface exchange coefficients and a revised steady-state model incorporating eye dynamics. *J. Atmos. Sci.*, **52**, 3969–3976.
- , 2000: A statistical analysis of tropical cyclone intensity. *Mon. Wea. Rev.*, **128**, 1139–1152.
- Fairall, C. W., J. D. Kepert, and G. J. Holland, 1994: The effect of sea spray on surface energy transports over the ocean. *Global Atmos. Ocean Syst.*, **2**, 121–142.
- Fiedler, B. H., 1994: The thermodynamic speed limit and its violation in axisymmetric numerical simulations of tornado-like vortices. *Atmos.–Ocean*, **32**, 335–359.
- , and R. Rotunno, 1986: A theory for the maximum windspeeds in tornado-like vortices. *J. Atmos. Sci.*, **43**, 2328–2340.
- Frank, W. M., and E. A. Ritchie, 1999: Effects of environmental flow upon tropical cyclone structure. *Mon. Wea. Rev.*, **127**, 2044–2061.
- , and —, 2001: Effects of vertical wind shear on the intensity and structure of numerically simulated hurricanes. *Mon. Wea. Rev.*, **129**, 2249–2269.
- Fulton, J. D., 2001: Insights into the hurricane vortex using a high resolution numerical simulation of Hurricane Bob (1991). M.S. thesis, Colorado State University, 84 pp.
- Gray, S. L., 1998: Analysis of the eyes formed in simulated tropical cyclones and polar lows. *Quart. J. Roy. Meteor. Soc.*, **124**, 2357–2375.
- Gray, W. M., 1968: Global view of tropical disturbances and storms. *Mon. Wea. Rev.*, **96**, 669–700.
- Guinn, T. A., and W. H. Schubert, 1993: Hurricane spiral bands. *J. Atmos. Sci.*, **50**, 3380–3403.
- Halliday, D., and R. Resnick, 1988: *Fundamentals of Physics*, 3d ed. John Wiley and Sons, 977 pp.
- Hausman, S. A., 2001: Formulation and sensitivity analysis of a non-hydrostatic, axisymmetric tropical cyclone model. Atmospheric Science Paper 701, Dept. of Atmospheric Science, Colorado State University, 210 pp.
- Heisler, H., 1995: *Advanced Engine Technology*. Arnold, 794 pp.
- Holton, J. R., 1992: *An Introduction to Dynamic Meteorology*. 3d ed. Academic Press, 511 pp.
- Hoskins, B. J., and F. P. Bretherton, 1972: Atmospheric frontogenesis models: Mathematical formulation and solution. *J. Atmos. Sci.*, **29**, 11–37.
- Jacob, S. D., L. K. Shay, A. J. Mariano, and P. G. Black, 2000: The 3D oceanic mixed layer response to Hurricane Gilbert. *J. Phys. Oceanogr.*, **30**, 1407–1429.
- Jin, D. Z., and D. H. E. Dubin, 1998: Regional maximum entropy theory for vortex crystal formation. *Phys. Rev. Lett.*, **80**, 4434–4437.
- Jones, S. C., 1995: The evolution of vortices in vertical shear. I: Initially barotropic vortices. *Quart. J. Roy. Meteor. Soc.*, **121**, 821–851.
- Jordan, C. L., 1958: Mean soundings for the West Indies area. *J. Meteor.*, **15**, 91–97.
- Kleinschmidt, E., 1951: Grundlagen einer Theorie der Tropischen Zyklonen (Basic principles for a theory of tropical cyclones). *Arch. Meteor. Geophys. Bioklimatol.*, **A4**, 53–72.
- Klemp, J. B., and R. B. Wilhelmson, 1978: The simulation of three-dimensional convective storm dynamics. *J. Atmos. Sci.*, **35**, 1070–1096.
- Knutson, T. R., and R. E. Tuleya, 1999: Increase hurricane intensities with CO₂-induced warming as simulated using the GFDL hurricane prediction system. *Climate Dyn.*, **15**, 503–519.
- Kossin, J. P., and M. D. Eastin, 2001: Two distinct regimes in the kinematic and thermodynamic structure of the hurricane eye and eyewall. *J. Atmos. Sci.*, **58**, 1079–1090.
- , and W. H. Schubert, 2001: Mesovortices, polygonal flow patterns, and rapid pressure falls in hurricane-like vortices. *J. Atmos. Sci.*, **58**, 2196–2209.
- LeeJoice, R. N., 2000: Hurricane inner-core structure as revealed by GPS dropwindsondes. M.S. thesis, Colorado State University, 56 pp.
- Lilly, D. K., 1962: On the numerical simulation of buoyant convection. *Tellus*, **14**, 148–172.
- Liu, Y., D.-L. Zhang, and M. K. Yau, 1999: A multiscale numerical study of Hurricane Andrew (1992). Part II: Kinematics and inner-core structures. *Mon. Wea. Rev.*, **127**, 2597–2616.
- Lorenz, R. D., J. I. Lunine, P. G. Withers, and C. P. McKay, 2001: Titan, Mars and Earth: Entropy production by latitudinal heat transport. *Geophys. Res. Lett.*, **28**, 415–418.
- Malkus, J. S., and H. Riehl, 1960: On the dynamics and energy transformations in steady-state hurricanes. *Tellus*, **12**, 1–20.
- Malkus, W. V. R., and G. Veronis, 1958: Finite amplitude cellular convection. *J. Fluid Mech.*, **4**, 225–260.
- McIntyre, M. E., 1992: Isentropic distributions of potential vorticity and their relevance to tropical cyclone dynamics. *Tropical Cyclone Disasters: Proceedings of ISCU/WMO International Symposium*, J. Lighthill et al., Eds., Peking University Press, 143–156.

- Michalke, A., and A. Timme, 1967: On the inviscid instability of certain two-dimensional vortex-type flows. *J. Fluid Mech.*, **29**, 647–666.
- Möller, J. D., and M. T. Montgomery, 2000: Tropical cyclone evolution via potential vorticity anomalies in a three-dimensional balance model. *J. Atmos. Sci.*, **57**, 3366–3387.
- , and L. J. Shapiro, 2002: Balance contributions to the intensification of Hurricane Opal as diagnosed from a GFDL model forecast. *Mon. Wea. Rev.*, **130**, 1866–1881.
- Montgomery, M. T., and R. J. Kallenbach, 1997: A theory for vortex Rossby-waves and its application to spiral bands and intensity changes in hurricanes. *Quart. J. Roy. Meteor. Soc.*, **123**, 435–465.
- , V. A. Vladimirov, and P. V. Denissenko, 2002: An experimental study on hurricane mesovortices. *J. Fluid Mech.*, **471**, 1–32.
- O'Brien, D. M., 1997: A yardstick for global entropy flux. *Quart. J. Roy. Meteor. Soc.*, **123**, 243–260.
- Ooyama, K. V., 2001: A dynamic and thermodynamic foundation for modeling the moist atmosphere with parameterized microphysics. *J. Atmos. Sci.*, **58**, 2073–2102.
- Ozawa, A., and H. Ohmura, 1997: Thermodynamics of a global-mean state of the atmosphere: A state of maximum entropy increase. *J. Climate*, **10**, 441–445.
- Paltridge, G. W., 2001: A physical basis for a maximum thermodynamic dissipation of the climate system. *Quart. J. Roy. Meteor. Soc.*, **127**, 305–313.
- Persing, J., M. T. Montgomery, and R. E. Tuleya, 2002: Environmental interactions in the GFDL hurricane model for Hurricane Opal. *Mon. Wea. Rev.*, **130**, 298–317.
- Roll, H. V., 1965: *Physics of the Marine Atmosphere*. Academic Press, 426 pp.
- Rotunno, R., and K. A. Emanuel, 1987: An air–sea interaction theory for tropical cyclones. Part II: Evolutionary study using a non-hydrostatic axisymmetric numerical model. *J. Atmos. Sci.*, **44**, 542–561.
- Sawada, Y., 1981: A thermodynamic variational principle in nonlinear non-equilibrium phenomena. *Prog. Theor. Phys.*, **66**, 68–76.
- Schechter, D. A., D. H. E. Dubin, K. S. Fine, and C. F. Driscoll, 1999: Vortex crystals from 2D Euler flow: Experiment and simulation. *Phys. Fluids*, **11**, 905–914.
- Schubert, W. H., M. T. Montgomery, R. K. Taft, T. A. Guinn, S. R. Fulton, J. P. Kossin, and J. P. Edwards, 1999: Polygonal eyewalls, asymmetric eye contraction, and potential vorticity mixing in hurricanes. *J. Atmos. Sci.*, **56**, 1197–1223.
- , S. A. Hausman, M. Garcia, K. V. Ooyama, and H.-C. Kuo, 2001: Potential vorticity in a moist atmosphere. *J. Atmos. Sci.*, **58**, 3148–3157.
- Shapiro, L. J., 1983: The asymmetric boundary layer flow under a translating hurricane. *J. Atmos. Sci.*, **40**, 1984–1998.
- Shay, L. K., A. J. Mariano, S. D. Jacob, and E. H. Ryan, 1998: Mean and near-inertial ocean current response to Hurricane Gilbert. *J. Phys. Oceanogr.*, **28**, 858–889.
- Smagorinsky, J., 1963: General circulation experiments with the primitive equation. I: The basic experiment. *Mon. Wea. Rev.*, **91**, 99–164.
- Smith, R. K., 2003: A simple model for the hurricane boundary layer. *Quart. J. Roy. Meteor. Soc.*, **129**, 1007–1027.
- Stephens, G. L., and D. M. O'Brien, 1993: Entropy and climate. I: ERBE observations of the entropy production of the earth. *J. Roy. Meteor. Soc.*, **119**, 121–152.
- Wang, Y., 2002a: Vortex Rossby waves in a numerically simulated tropical cyclone. Part I: Overall structure, potential vorticity, and kinetic energy budgets. *J. Atmos. Sci.*, **59**, 1213–1238.
- , 2002b: Vortex Rossby waves in a numerically simulated tropical cyclone. Part II: The role in tropical cyclone structure and intensity changes. *J. Atmos. Sci.*, **59**, 1239–1262.
- , and G. J. Holland, 1996: The beta drift of baroclinic vortices. Part I: Adiabatic vortices. *J. Atmos. Sci.*, **53**, 411–427.
- Willoughby, H. E., 1990: Gradient balance in tropical cyclones. *J. Atmos. Sci.*, **47**, 265–274.
- , 1998: Tropical cyclone eye thermodynamics. *Mon. Wea. Rev.*, **126**, 1653–1680.
- , J. A. Clos, and M. G. Shoreibah, 1982: Concentric eye walls, secondary wind maxima, and the evolution of the hurricane vortex. *J. Atmos. Sci.*, **39**, 395–411.
- Yamasaki, M., 1983: A further study of the tropical cyclone without parameterizing the effects of cumulus convection. *Pap. Meteor. Geophys.*, **34**, 221–260.
- Zhang, D.-L., Y. Liu, and M. K. Yau, 2000: A multiscale numerical study of Hurricane Andrew (1992). Part III: Dynamically induced vertical motion. *Mon. Wea. Rev.*, **128**, 3772–3788.
- , —, and —, 2002: A multiscale numerical study of Hurricane Andrew (1992). Part V: Inner-core thermodynamics. *Mon. Wea. Rev.*, **130**, 2745–2763.